

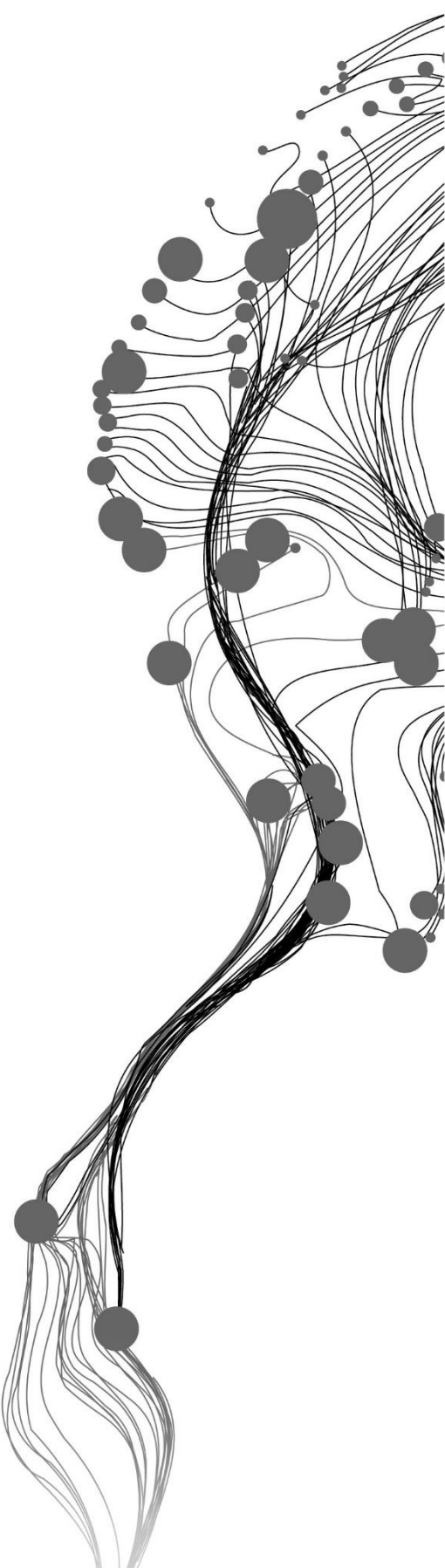
ANALYSING THE IMPACT OF RAINFALL AND SOIL MOISTURE CHARACTERISTICS ON ENHANCED RIVER DISCHARGE

CELESTE VIDAD

March, 2018

SUPERVISORS:

DR J. ETTEMA
DR D.P. Shrestha



ANALYSING THE IMPACT OF RAINFALL AND BASIN CHARACTERISTICS ON ENHANCED RIVER DISCHARGE

CELESTE VIDAD

Enschede, The Netherlands

March 2018

Thesis submitted to the Faculty of Geo-Information Science and Earth Observation of the University of Twente in partial fulfilment of the requirements for the degree of Master of Science in Geo-information Science and Earth Observation.

Specialization: Applied Earth Sciences

SUPERVISORS:

Dr. J. Ettema

Dr. D.P. Shrestha

THESIS ASSESSMENT BOARD:

Prof.Dr. V.G. Jetten (Chair)

Dr.Ir. C.M.M. Mannaerts (External Examiner, ITC Department of Water Resources)

DISCLAIMER

This document describes work undertaken as part of a programme of study at the Faculty of Geo-Information Science and Earth Observation of the University of Twente. All views and opinions expressed therein remain the sole responsibility of the author, and do not necessarily represent those of the Faculty.

ABSTRACT

The generation of an enhanced river discharge is product of catchment response to its soil moisture state and rainfall input. Soil moisture is an important characteristic of the catchment. However, it has high temporal and spatial variabilities which motivates the efforts of soil moisture remote sensing . Remote sensing allows the regular acquisitions of soil moisture state over a wide area.

An attempt to retrieve soil moisture from radar remote sensing is one of the objectives addressed in the study. However, due to catchment topography and sensor characteristics, a meaningful soil moisture map was not achieved through radar remote sensing. Another attempt to map the soil moisture in the area was to use the in-situ soil moisture values and catchment characteristics to create Boolean classes with mean soil moisture values. This resulted to a map showing soil moisture state of the study area during the wet season.

The derived soil moisture map approximated the field capacity values of the soil texture classes present in the area. To fulfil the third objective of analysing the effect of initial soil moisture conditions and rainfall input to the catchment response, an event-based model was used. Results from the event-based model shows that catchment can respond similarly to different rainfall inputs and initial soil moisture state. The simulation has also shown that fully saturated soil moisture conditions paired with low rainfall return period generates a larger discharge volume compared to a rainfall event with high return period and paired with non-saturated soil moisture conditions.

ACKNOWLEDGEMENTS

Jesus, my first love and deepest gratitude belongs to You.

To the faculty of ESA, I am very grateful for the knowledge and expertise imparted. To my supervisors, Janneke and Dhruva, I thank you for the guidance throughout this thesis process. Thank you for being encouraging and critical as you help me around issues I faced in doing the thesis. My heartfelt thanks to Dinnand who made arrangements for the ADPC internship and to Bart who is a constant source of support throughout the MSc program.

To the team at Asian Disaster Preparedness Center: Dr Peeranan, Dr Farrukh and Dr Mahmoud, thank you for the opportunity to intern at ADPC. To Dr Farrukh, thank you for the inputs on radar and functioning as my supervisor during the internship in Bangkok, to Ruamporn Moonjun of LDD and her colleagues who showed us around Khao Kho. To Dr Saranthip and Dr Korakod of Naresuan University and their students, Leak, Bwi and Dhamakar, thank you for the logistical support during the fieldwork and the hospitality you've provided during our stay in Naresuan. Thank you, many times over. Special thanks also to Juliet who shared Thailand experiences and her LiSEM database.

To my classmates in ESA and friends in ITC, my memories of ITC will not be the same without you. It was a joy to experience graduate studies together. To my family in Enschede, International Christian Fellowship, I praise the Lord when I remember you. Thank you for the friendship and warmth you've extended to all students who enter your doors. May the Lord bless you in all your works.

And to my Mother and Sister, thank you for encouraging me to finish the program. It couldn't happen without both of you.

TABLE OF CONTENTS

List of figures.....	iv
List of tables.....	v
Introduction.....	8
Background.....	8
Soil moisture retrieval from remote sensing.....	8
Hydrological modelling of soil moisture.....	9
Research problem.....	10
Objectives and questions.....	10
Thesis structure.....	10
Study area.....	11
Geographic location.....	11
Climate.....	11
Geomorphologic setting.....	12
Land use and land cover.....	13
Historical hazards.....	14
Methodology.....	15
Data collection.....	15
Radar data processing.....	16
Rainfall analysis.....	18
Rainfall-runoff modelling using LiSEM.....	19
Soil moisture measurement and radar retrieval.....	26
Soil moisture based on in-situ data.....	26
Soil moisture based on radar-remote sensing.....	30
LiSEM Analysis.....	33
Results of model calibration.....	33
Catchment response to change in land cover.....	34
Response to various initial soil moisture.....	38
Similar catchment response to different rainfall vent.....	39
Simulation of hazard event.....	42
Conclusions and Recommendations.....	43
References.....	45
Annex A.....	48
Annex B.....	50

LIST OF FIGURES

2.1 Location map of study area.....	11
2.2 Mean monthly temperature and rainfall.....	12
2.3 Land cover map	13
3.1 Sample location map.....	14
3.2 Gumbel extreme value analysis	19
3.3 Soil map.....	22
3.4 Soil texture.....	22
3.5 Box plot of Ksat values	23
3.6 Box plot of porosity	23
3.7 Flowchart of methodology.....	25
4.1 Location map of soil moisture measurements.....	26
4.2 Box plot of soil moisture versus slope.....	28
4.3 Box plot of soil moisture versus land use.....	28
4.4 Box plot of soil moisture versus soil texture.....	28
4.5 Soil moisture using Boolean method	29
4.6 Mean and standard deviation backscatter.....	30
4.7 Soil moisture map based on radar remote sensing.....	31
4.8 Validation of radar-retrieved soil moisture.....	31
4.9 Box plot of slope gradient and backscatter standard deviation	32
5.1 Hydrograph of hydrological calibration.....	33
5.2 Sub-catchments of Namchun.....	35
5.3 2016 Land cover	35
5.4 2000 Land cover	35
5.5 Grassland and cropland to forest cover.....	35
5.6 Catchment response at Outlet 1 of two different land cover.....	36
5.7 Catchment response at Outlet 2 of two different land cover.....	36
5.8 Catchment response at Outlet 1 to different rainfall events	37
5.9 Catchment response at Outlet 1 for different initial soil moisture.....	39
5.10 Hydrograph of catchment response to 10YR WP and 5YR FC	39
5.11 Hydrograph of catchment response to 20YR WP and 10 YR FC	40

5.12 Hydrograph of catchment response to 50YR WP and 20YR FC	40
5.13 Hydrograph of 2YR FS and 50YR FC.....	42

LIST OF TABLES

3.1 Sensor dataset characteristics.....	17
3.2 Maximum daily rainfall	19
3.3 Main data used in database generation.....	21
3.4 Parameters required by LISEM.....	21
3.5 Soil data characteristics	23
3.6 Box plot of ksat and porosity	23
3.7 Scenarios run in LISE,.....	24
4.1 Statistics of slope gradient and soil moisture	27
4.2 Statistics of land use units and soil moisture.....	27
4.3 Statistics of soil texture and soil moisture	27
4.4 Results of Boolean operation	28
5.1 Measured data at Namhun Outlet from 2005.....	33
5.2 Calibration factors used in the model	34
5.3 Land cover change matrix.....	34
5.4 Summary of catchment response due to land cover change	37
5.5 Comparisons of peak discharge of 2YR FC in 2000 return rainfall events in 2016	37
5.6 Summary of various initial soil moisture conditions.....	38
5.7 Catchment response to 10YR WP and 5YR FC	39
5.8 Catchment response to 20YR WP and 10YR FC	40
5.9 Catchment response to 50YR WP and 20YR FC	40
5.10 Catchment response to 2YR FS and 50YR FC.....	41

1. INTRODUCTION

1.1 Background

Flood hazards affect more people than any other hazard worldwide (UNISDR, 2015). In Asia, 35% of recorded disasters since the start of the 20th century is attributed to a flooding event, and 68% of these flood events occurred in South Asia and Southeast Asia Region (CRED, 2017). Using the estimates from CRED (2017), flood disasters in Southeast Asia have caused approximately 57 billion USD in damages and affected more than 100 million people since the start of the 21st century. The flood disasters in the region are mainly triggered by considerable rainfall input due to monsoons (Loo et al., 2015).

Flood event in a catchment typically originates from excess runoff, produced from the inability of soil to absorb all of rainfall amount that reaches the ground surface. Depending on the characteristic of the rainfall event in terms of amount, intensity and duration, surface runoff is generated in two conditions. 1) High intensity short duration rainfall event exceeds the infiltration capacity of the soil or 2) Amount of rainfall exceeds the storage capacity of the soil. The former conditions create a Hortonian overland flow while the latter creates saturated overland flow.

The occurrence of flooding is not only a function of rainfall amount and intensities but also of factors that impact the infiltration and storage capacity of the soil. Infiltration controls the conversion of the amount of precipitation into runoff. During a rainfall event, infiltration capacity is determined by the rainfall intensity and hydraulic conductivity (Dingman, 1994). The soil hydraulic conductivity is affected by physical properties of soil such as grain size, grain size distribution and soil structure. These properties determine the downward flow of water through the soil. At the surface, organic matter content also affects the hydraulic conductivity. Land use changes caused by human activities affect the interstitial space between soil particles resulting to reduced soil porosity and increased compaction. Changes in soil structure may lead to diminished soil hydraulic conductivity (Dunne, 1983). The antecedent moisture conditions regulate the amount of additional water the soil can accommodate, affecting the amount of water which is converted to runoff.

The significance of soil moisture in catchment studies lies on its role in surface runoff generation. Generation of surface runoff is a threshold process that is highly influenced by wetness conditions which are effectively controlled by weather and soil moisture storage of the catchment (Penna et al., 2011). Soil moisture conditions could be highly variable in its temporal and spatial distribution. Hydrometeorological processes of evapotranspiration and precipitation affects and is mutually influenced by soil moisture (Entekhabi et al., 1996). This phenomenon is responsible for the temporal variability of soil moisture. At the same time, soil moisture is also affected by topography, soil physical properties, vegetation and land use (Moran et al., 2004), which are spatially variable over the catchment. The importance of soil moisture as water storage and its high variability required monitoring.

1.2 Soil moisture retrieval from remote sensing

Due to limits in spatial coverage as well as the economic cost of installing and maintaining in-situ networks, it is unsuitable to use in-situ methods to large areal coverage. Remote sensing provides a solution to this issue by covering large swaths of space at regular time periods. Microwave methods of remote sensing is sensitive to soil moisture. Microwave remote sensing can be distinguished into two types: passive and active sensors. Sensors with passive microwave function deployed for soil moisture monitoring include Advanced Microwave Scanning Radiometer (AMSR-E), Soil Moisture and Ocean Salinity (SMOS), Hydrospheric States (HYDROS) and Soil Moisture Active/Passive (Aqua EOS, n.d; SMOS ESA, n.d; Entekhabi et al. 2004; SMAP NASA, n.d). Most passive microwave sensors use low frequencies associated with the L-Band

due to its low signal-to noise-ratio (Velde, et al., 2015) and better penetration through vegetated canopy. Despite the fine temporal resolution of radiometers (3 days revisit time), remote sensing data from these sensors are obtained at coarse spatial resolutions (10km for AMSR-E and 35 km for SMOS) which limits their direct application to scales at which hydrological processes are simulated.

Active microwave sensors, particularly Synthetic Aperture Radar (SAR) offer a finer resolution soil moisture product at less than 100m at resolutions of 7-24 day-revisit time. The backscatter detected by the sensor is a function of incidence angle, polarization, wavelength, surface roughness and dielectric properties of soil and vegetation (Moran et al., 2004). Soil moisture retrieval methods were developed in order to decouple the effect of satellite signal properties, surface roughness, vegetation and soil moisture to the backscatter coefficient. The parametrization of surface roughness and vegetation is important in retrieving soil moisture from SAR data (Kornelsen & Coulibaly, 2013).

The assimilation of remotely sensed soil wetness into hydrologic modelling of the catchment are mostly done in kilometer-wide resolutions. This approach has been conducted in hydrologic modelling of homogenous response units and not for fully distributed models mainly because of constrains in the spatial resolution. With the launch of Sentinel 1 and its higher temporal and spatial resolution, many researchers have projected the positive impact of its finer radiometric capabilities in soil moisture retrieval [(Wagner, et.al., 2009), (Doubková, et.al., 2012), (Malenovský et al., 2012), (Das & Paul, 2015), (Balenzano et al., 2013) and (Zribi et al., 2014)].

The variability of soil moisture can be monitored at catchment wide scale through: 1) satellite remote sensing technology and 2) continuous simulation (Seneviratne et al., 2010). However, certain capabilities of available passive and active sensors are limited when it comes to soil moisture estimation at the catchment scale (Kornelsen & Coulibaly, 2013; Velde et al., 2015). The constraints of remote sensing method can be supplemented with data integration by using a hydrological model. Hydrological models simulate otherwise unobserved processes within the watershed and how catchment characteristics in turn affect these processes (Kornelsen & Coulibaly, 2013; Moran et al., 2004; Entekhabi et al., 1996).

1.3 Hydrological modelling of soil moisture for rainfall-runoff response

Soil moisture estimation through modelling is another method for retrieving soil moisture values temporally and spatially. Where remotely sensed soil moisture allows measurement of actual wetness of catchment at varying time and scales, their soil moisture retrieval capabilities are also limited through sensor imperfections and characteristics of target parameters (Das & Paul, 2015). The resulting values from modelling methods are considered useful in initializing the catchment conditions for hydrological simulations.

Hydrologic modelling can be classified as either continuous or event-based (Berthet et. al., 2009). Continuous models rely on larger time steps to simulate processes in catchment conditions. Continuous models are highly applicable for long-term impacts of hydrological changes and watershed management practices (Borah et al., 2007). The reverse is true for event-based models which simulate catchment conditions in relation to a single rainfall event. because event-based models simulate catchment only during a rainfall event, it requires rainfall intensities at smaller timesteps. This also means it does not account for evaporation and transpiration processes that occur in the catchment.

The nature of event-based simulations makes it suitable in determining the impact of initial soil moisture conditions to rainfall-runoff processes and resulting outlet discharge. The fine temporal resolution allows the characterization of the catchment response to the rainfall event through the peak discharge, total discharge and peak time values.

1.4 Research problem

The study area in Thailand had a flashflood event in 2001 causing fatalities and damages downstream of the flashflood source. The generation of a potential flood event is attributed to catchment response to rainfall input and soil moisture conditions. Catchment response to rainfall is influenced by its soil properties which regulate infiltration and amount of moisture storage in the soil. In order to forecast catchment response to rainfall events, knowledge about its initial soil moisture state is crucial. This study will deal with two issues: 1) the extent of the influence of catchment characteristics on the variability of soil moisture and 2) the effect of varying initial soil moisture conditions and rainfall characteristics to the generation of enhanced river discharge.

1.5 Objectives and questions

General objective: To analyze the impact of soil moisture conditions on enhanced river discharge and flash flood events in the Nam Chun watershed, Thailand

Research objectives are as follows:

Research objective 1: Assess the accuracy of radar-derived soil moisture map

Research objective 2: Identify the contribution of catchment properties to spatial variability of soil moisture

Research objective 3: Assess how various initial soil moisture conditions contribute to a catchment response using an event-based hydrological model

Research questions are as follows:

- What factors affect the accuracy of the soil moisture map from SAR?
- What is the impact of topography to soil moisture?
- What is the impact of land use/land cover to soil moisture?
- What catchment property contributes the most to variance of soil moisture values?
- What is the response of the catchment in terms in terms of peak discharge, total discharge and peak time to an extreme rainfall event given the driest soil moisture condition?
- What is the response of the catchment to rainfall with low return period given the wettest soil moisture condition?

1.6 Thesis structure

Chapter 2 of the thesis presents the study area, Chapter 3 provides the methodology of the study, including the inputs required for the simulation, Chapter 4 presents the results of soil moisture measured from the field and the results of soil moisture retrieval using radar, Chapter 5 presents the results of LISEM simulations and Chapter 6 presents the conclusions and recommendations of the study.

2. STUDY AREA

2.1 Geographic location

The study is focused on the Namchun watershed located in Phetchabun Province of Central Thailand. Based on WGS 1984 projection, the study area lies 16°40' - 16°50' north latitude and 101°0' - 101°9' east longitude. The watershed is approximately 70 km² in area with recorded elevation between 180 m – 1490 m above sea level. Figure 2.1 illustrates the geographic location of the catchment with inset of its location within Phetchabun (bottom right inset) and location of Phetchabun within Thailand (upper right inset).

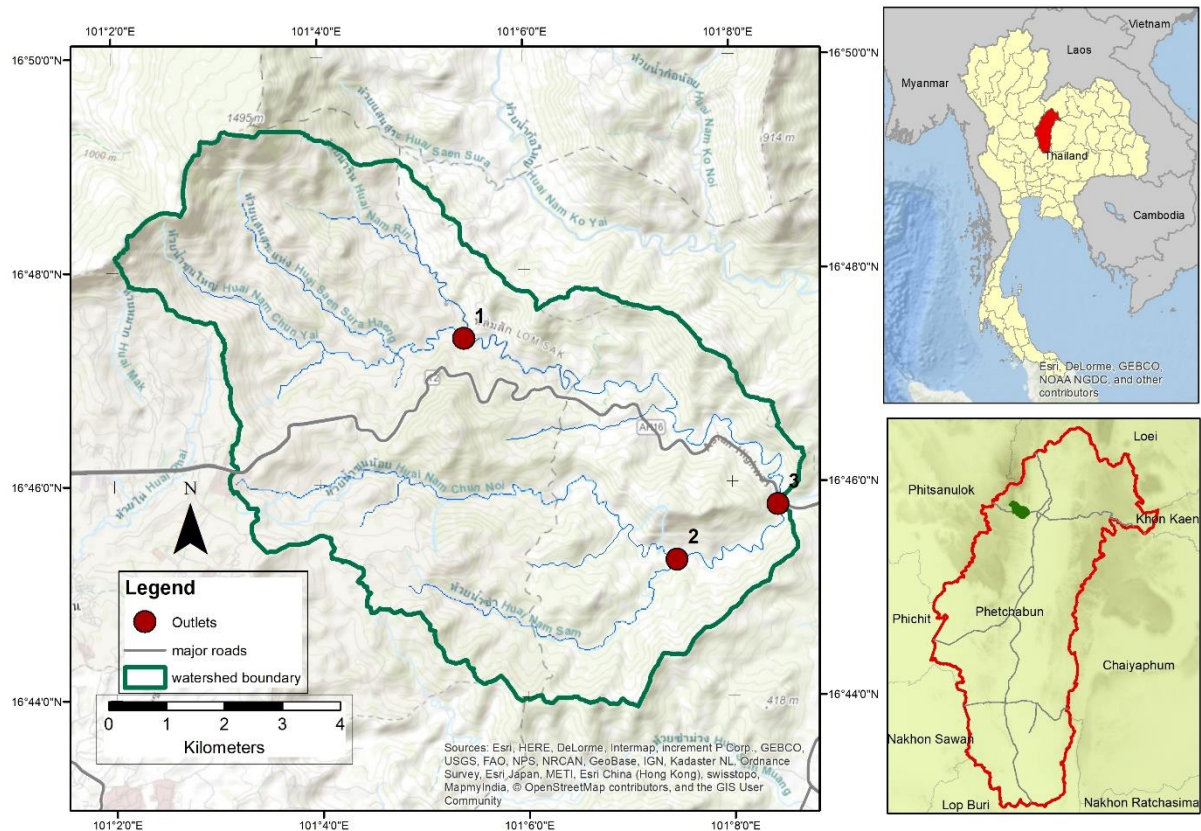


Figure 2.1. Location map of study area.

2.2 Climate

The climate of Thailand is characterized as equatorial with dry summer. This classification refers to conditions where temperatures are above 18°C throughout the year and rainfall during the warmer months are less than 60mm. Thailand climate is dominated by the southwest and northeast monsoons.

The southwest monsoon originates from the Indian Ocean, bringing in warm, moist air which causes the abundant rainfall observed from May – September. The northeastern monsoon originates from Mainland China and brings with it cold dry air which is responsible for the dry season observed from October – February. Average annual rainfall in the study area based on a 65-year record (1952-2016) is 1062 mm. The mean temperature over one year based on a 17-year record (2000-2016) is 25.7°C. Figure 2.2 illustrates rainfall and temperature values per month over a 12-month period.

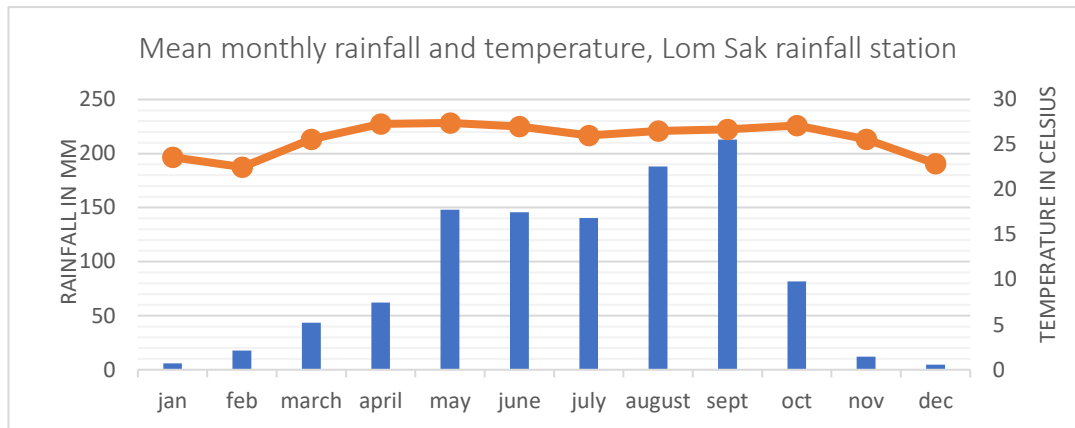


Figure 2.2. Mean monthly rainfall and temperature in the study area based from measurements at Lom Sak Rainfall station.

2.3 Geomorphologic setting

The Phetchabun massif is composed of a pair of north-south trending mountain range which is separated by the Pa Sak river valley. The pair of mountain ranges are part of the larger Loei-Phetchabun-Nakhon Nayok belt that extends from northern Laos towards central Thailand. The eastern mountain range forms a significant watershed divide between the basins of Chao Phraya and Mekong River. Towards southeast of the massif is the Khorat Basin, also known as the Khorat Plateau which comprises the northeastern region of Thailand (Lofile, E., Kubionok, 1996).

Namchun watershed is part of the hillslopes of the western Phetchabun mountain range. Towards west of the watershed leads to higher elevation and undulating slopes of the mountain range. Towards the north and south are the rugged hillslopes of the mountain range and towards east is the Pa Sak river valley. Discharge out of the Namchun watershed drains to a tributary of the Pa Sak River. The Pa Sak River drains towards the Chao Phraya River.

The area can be classified rugged based on the distribution of its slope gradients. Areas where slope gradient is less than 5 degrees are present in less than 2% of the study area and mainly observed in riverbeds. Moderate gradients between 5-20 degrees and steep gradients between 21-40 degrees are present at 37% and 58% of the study area, respectively. Gradients above 40 degrees compose less than 3% of the study area

Namchun is composed of two smaller sub-catchments. The sub-catchments are divided by a range oriented northwest-southeast. The northern sub-catchment is characterized by steep slopes and located in the higher elevations. The southern sub-catchment is characterized by moderate slopes in its uppermost part and by steep slopes in areas closer to the outlet. To distinguish between the two sub-catchments, the outlet point of the northern sub-catchment is labelled Outlet 1 and the outlet point of the southern sub-catchment is labelled Outlet 2. The main discharge point of Namchun is labelled Outlet 3. Figure 2.1 shows the location of these outlet points.

2.4 Land use and land cover

Land cover in Namchun catchment is mainly distributed over forest land, cropland, man-made water reservoir and builtup areas. Land use consists primarily of forested land and agrarian land. Use of agrarian land is divided between orchards and cultivated crops. Orchards in Namchun are dedicated to cultivating tamarind, teak and rubber. Cultivated crops in the area are rice, maize, ginger, cassava and cabbages. A water reservoir was established within the central part of the catchment for irrigation purposes downstream of the watershed after Year 2005. Figure 2.4 shows the land cover map of 2016 from Asian Disaster Preparedness Center. The major land cover types observed and their location within the watershed are shown in the figure.



Figure 2.3. Land cover types in Namchun watershed. (Clockwise from top) Forest cover as seen from the highway (camera facing north-northwest); Photo from the dam of the water reservoir (camera facing northwest) ; Cropland that was left to fallow after maize harvest; Cropland used to cultivate paprika (in the foreground) and rice (in the background); Forest cover imaged from the ground; Cropland used to cultivate cabbages located at the edge of forested area (camera facing southeast). (Center) 2016 Land cover map of Namchun watershed.

2.5 Historical hazards

A hazard event characterized by flash flood and debris flow was recorded in 11 August 2001 in Nam Ko Yai Village. The hazard event translated into a disaster event when it caused 136 casualties and 5 million USD in economic damages. The Nam Ko Yai catchment is an adjacent catchment of Namchun and is also a sub-catchment of Pa Sak River.

Rainfall record from Lom Sak rainfall station shows that maximum daily rainfall during the 2-week period that precedes the hazard event was less than 36 mm. Based on 1952-2016 record, 36mm rainfall has a recurrence interval of 1.5 years which can be considered normal rainfall amount (see Chapter 3.3 for further discussion of how the recurrence interval of rainfall depths were determined). However, 9 days of continuous rain with accumulate 104 mm rainfall amount were recorded before the debris flow event which could have also triggered the hazard. An investigative study in the area succeeding the disaster event conclude that elevated rainfall is not the direct cause of debris flows and flashflood. Rather, the event could have been more likely triggered by the prolonged rainfall, saturated soils, steep terrain and changes in the land cover (Yumuang, 2006).

3. METHODOLOGY

This chapter is divided between data collection, data processing and preparation of simulation input database. Data processing can be further classified between works applied in radar data and rainfall data. The final section of the chapter discusses the generation of input maps for event-based modelling. The overall workflow of the study is provided in the last part of the chapter in Figure 3.7.

3.1 Data collection

Field work was conducted from 15 September – 24 September 2017. Information pertaining to soil hydraulic conductivity, soil moisture, porosity, texture and land use were collected during this period. Information related to rainfall and land use were also collected from relevant government agencies in Thailand. Soil data was collected to obtain values for input in the simulation as well as to validate the accuracy of retrieved soil wetness values from radar remote sensing. The location of soil sample points are presented in Figure 3.1.

Soil moisture and disturbed soil sampling

Thirty disturbed soil samples and sixty soil moisture readings were collected from different areas within the catchment. Twenty soil moisture readings were also obtained in a flat grassland outside of the catchment to serve as control for estimating the wetness from radar remote sensing.

Soil moisture data was collected using gravimetric and electric conductivity measurements. Gravimetric approach in measuring soil moisture involves collecting soil sample at approximately 200 grams from the upper 5 cm of the soil profile and stored in a sealed container. The difference between the wet weight and desiccated weight of the sample, multiplied to the soil bulk density gives the volumetric soil moisture content. The handheld equipment for electric conductivity measurement generates a 20 MHz signal in its pointed rods, producing a tiny electromagnetic field within the sampling area allowing the instrument to measure soil moisture through pore water conductivity. The gravimetric soil moisture serves as calibration data for the handheld sensor. The correlation of soil moisture values from the two methods are presented in the annex.

Undisturbed soil sampling and processing

Sixteen undisturbed samples were collected for purpose of measuring hydraulic saturated conductivity (k_{sat}), porosity and bulk density. A soil core sampler that is 2.5 cm in radius and 5 cm in height was used for undisturbed soil sampling. The soil samples were then stored in a sealed cylindrical casing with the same dimensions as the core sampler to minimize moisture loss and to keep the sample in its 'in-situ' state.

Soil samples were weighted and submerged in a water bath in the laboratory for 24 hours to saturate all voids. The samples were afterwards subjected to a permeameter setup to determine k_{sat} . Samples were afterwards heated in an oven to remove its moisture content before its bulk density and porosity could be measured.

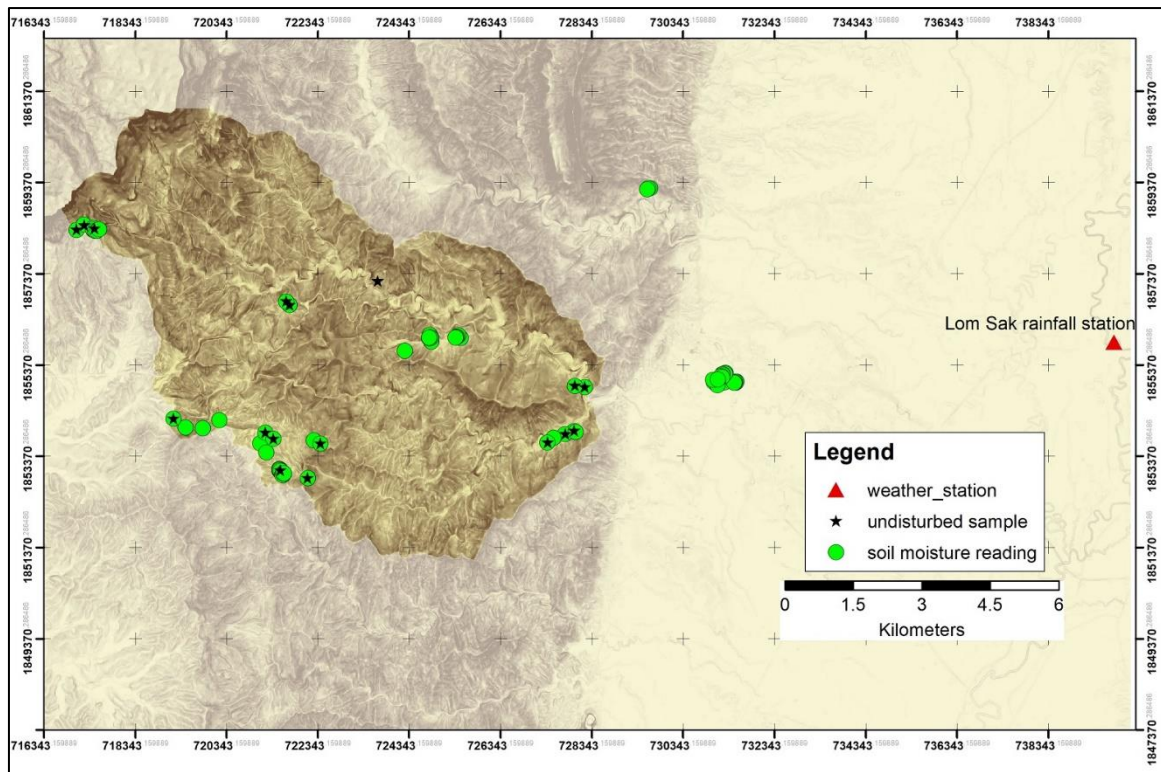


Figure 3.1 Location map of sampling points in the study area

3.2 Radar Data Processing

An objective of the study is to assess the accuracy of radar-derived soil moisture in the catchment. This objective entailed retrieval of soil wetness from radar backscatter which was acquired over a one-year period from October 2016 – September 2017

3.2.1 Description of sensor

The data used in this study was derived from the synthetic aperture radar onboard the two Sentinel 1 satellites of the European Space Agency (ESA). The radar instrument operates at the C-band at frequency of 5.405 GHz with a right-looking active phased array antenna. The retrieved data are in interferometric wide (IW) swath mode sensed at 30.9°-40.6° incidence angle and polarized along the VV and VH channels. IW swath mode is the default acquisition mode of Sentinel 1 over terrain surfaces. The selected data were processed until Level 1 ground range detected (GRD) which are multi looked (5 looks in range orientation and 1 look in azimuth orientation) and data is projected to ground range using an ellipsoid model. Radar images processed at this level have a resolution of 20mx22 m and presented at 10 m pixel spacing. Table 3.1 gives a summary of the sensor characteristics.

3.2.2 Description of dataset

The temporal period selected for this study is from October 2016 – September 2017. A total of 63 images were sensed by the instrument during this period. The satellite constellation allows an average revisit time of 6 days over the sensing period. A description of individual radar image is included in the annex of this thesis.

Sentinel 1 dataset characteristics	
Mode	Interferometric wide
Swath width	250 km
Polarization	VV, VH
Number of looks (range x azimuth)	5x1
Range x azimuth resolution	20x22 meters
Incidence angle	30.9°- 46.0°

Table 3.1 Properties of dataset that was retrieved from Sentinel 1

3.2.3 Description of methodology

A. Pre-processing of radar images

All acquired radar images were preprocessed using the open-source Sentinel Application Platform Toolbox (SNAP). Backscattering coefficient of pre-processed radar images are expressed in units of decibels. The images used in radar processing are all oriented in the VV polarization.

Pre-processing involved four steps:

1. Radiometric calibration – in order to convert DN values of raw images into backscattering coefficients (σ^0);
2. Speckle reduction – speckle is reduced by multi-look processing, which is a feature of Level 1 ground range detected processing; in this study, speckle is further reduced by using Lee filtering;
3. Terrain correction – geometric correction was applied using the Shuttle Radar Topography Mission (SRTM) Digital Elevation Model at 3 arc seconds.

B. Change detection method

Change detection to retrieve soil moisture is a suitable method considering the multi-temporal dataset that is available. This approach operates on the assumption that changes in radar backscatter can be attributed to causes acting on different time scales. Long term changes are caused by change in land cover, mid-term changes are due to vegetation phenology and short-term changes are caused by variation in soil moisture. This method requires time series data of the study area, matching spatial resolutions of the radar images, radiometrically calibrated, geo-coded and co-registered dataset.

With short time intervals between the image acquisitions in the dataset, short-term changes are captured. Because of the short intervals in acquisition, the changes in radar backscatter are attributed to changes in moisture content in the soil surface. For soil moisture retrievals, a dry reference image is required which will be subtracted from image of interest. Because the image represents dry conditions, soil moisture is minimal and radar backscatter that is present is attributed to roughness and vegetation characteristics. The difference between the image of interest and dry reference image represents the wetness state of the study area which is still expressed as radar backscatter.

The wet reference image represents radar backscatter values when conditions are wettest. The difference between the wet reference image and dry reference image gives the radar backscatter value of maximum soil wetness. By rationalizing the radar backscatter of wetness state from a particular date over the backscatter value of maximum soil wetness, the degree of saturation of soil surface is obtained. This degree of saturation is hereafter referred to as the soil wetness index (SWI). Because radar waves are limited in its penetration of the soil surface, SWI can only refer to the wetness state of the upper 5 cm of the soil profile.

SWI is an indication of the saturation of available pore spaces in the soil layer and ranges from 0 to 1 (0 signifying dry conditions and 1 for wet conditions). From the radar stack, mean and standard deviation backscatter values were calculated per pixel and were used to determine the dry reference image (σ^0_{dry}) and

wet reference image (σ_{wet}^0). Dry backscatter is determined as 2 standard deviation values subtracted from the mean value per pixel ($\mu_{x,y}$) while the wet backscatter is two standard deviation added to the mean value per pixel.

SWI retrieval can be expressed as:

$$\text{SWI}_t \in [0, 1] = \frac{\sigma_t^0 - \sigma_{\text{dry}}^0}{\sigma_{\text{wet}}^0 - \sigma_{\text{dry}}^0} \quad (1)$$

$$\text{Where } \sigma_{\text{wet}}^0 = \mu_{(x,y)} + 2 * \text{SD}_{(x,y)} \quad (2)$$

$$\sigma_{\text{dry}}^0 = \mu_{(x,y)} - 2 * \text{SD}_{(x,y)} \quad (3)$$

The method presented here is an adoption of change detection approach applied to ASCAT (Advanced Scatterometer) at 25 km resolution (Wagner, et.al., 2009). This method was applied in a semiarid region in by Zribi in 2014 where soil moisture retrieval correlated with in-situ soil moisture at $R^2=0.50$. Adoption of this method particularly for Sentinel data was proposed by Hornacek et al., in 2012 in the context of soil moisture monitoring, taking advantage of the high temporal acquisition capabilities of Sentinel 1.

3.3 Rainfall analysis

Available rainfall data within catchment proximity was retrieved from Lom Sak Meteorological Station, located 10 km east of the Namchun watershed. Figure 3.1 shows the location of Lom Sak Meteorological Station with respect to Namchun.

3.3.1 Recurrence interval of extreme events

Maximum daily rainfall for each year from 1952-2016 was retrieved from the Lom Sak dataset and a Gumbel distribution was applied on the maximum daily rainfall values. Gumbel is a type of a type of extreme value distribution that represents distribution of maximum values. As shown in Figure 3.2, the Gumbel distribution succeeds in representing the recorded maximum events with a correlation coefficient above 0.97. The established relationship between daily rainfall and return period was used to determine the maximum daily rainfall of different return periods. Table 3.3 shows the maximum daily rainfall from different return periods.

3.3.2. Designing an extreme rainstorm event

Design storms were generated for the study area to evaluate the hydrologic response to different intensities of various storm return periods. A common method to create a design storm is to use intensity-duration-frequency (IDF) curves. Because the rainfall dataset from Lom Sak is limited to daily rainfall, an IDF curve for the study area is not possible. However, an IDF curve based on disaggregated 3-hour rainfall measurements from 1981-2010 in a rainfall station in Sukhumvit, Bangkok exists (Shrestha, 2017).

Using the IDF curve, the rainfall amount for a 24-hour duration was retrieved. The retrieved rainfall amounts using the IDF curve are greater than the maximum daily rainfall from Lom Sak Station. This implies that the amount of maximum daily rain per return event in the study area is within the range of the daily rainfall amount that can be possibly generated based on the IDF curve. Table 3.2 shows the computed rainfall intensity for a rainfall event with a 24 hour duration, based on the IDF curve and the rainfall amount it can generate.

Based on the IDF curves, rainfall intensity for particular time step for every return period can be calculated, and the known rainfall intensity with respect to rainfall duration, is used to compute for the rainfall depth. Incremental rainfall is determined using the differences between each successive precipitation depth.

Incremental rainfall per timestep is calculated until the cumulative rainfall equals that of the maximum daily rainfall derived from Gumbel. Maximum daily rainfall values for particular recurrence intervals are shown in Table 3.2. Finally an alternating block method was used to sort the intensities of the rainfall event. Design storm with 2, 5, 10, 20, 50-year recurrence intervals were created.

Return period	Max daily rainfall from Gumbel (mm)	Rainfall intensity for 24 hour duration (mm/h)	Rainfall amount based on IDF (mm)
1 in 2	79.3	5.0	120.8
1 in 5	108.8	7.5	178.8
1 in 10	128.0	8.5	203.3
1 in 20	147.0	10.1	242.4
1 in 50	171.1	11.2	269.8

Table 3.2 Comparison of max daily rainfall amount per return period based on Gumbel plot and retrieval from IDF

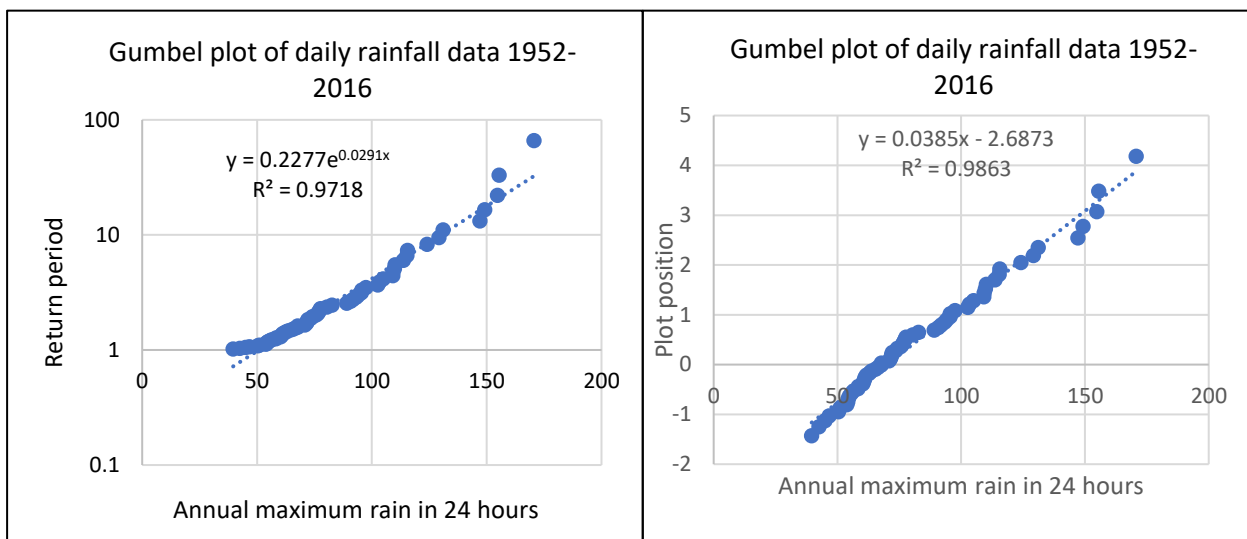


Figure 3.2. Fit of Gumbel extreme value distribution to recorded maximum rainfall events in Lom Sak station.

3.4 Rainfall-runoff modelling using LiSEM

One of the objectives of the study is to characterize catchment response with different initial soil moisture conditions to rainfall events with varying return periods. In fulfilling this objective, an event-based simulation was used to analyze the behavior of the catchment with respect to varying conditions in rainfall input and initial soil moisture.

LiSEM is physically based hydrologic model designed to simulate natural processes involved in rainfall-runoff interactions by operating based on water and sediment balance equations. LiSEM is also a fully distributed model meaning it runs on a pixel by pixel basis where each pixel has its own value, simulating likewise heterogeneities in a given catchment. The model does not consider evapo-transpiration and groundwater flow processes, instead it treats rainfall input as a single event. This makes LiSEM particularly useful in analyzing effects of soil cover and land use changes on runoff and erosion in a catchment given a rainfall event (De Roo, et al., 1996). Water balance processes of rainfall, interception, infiltration and surface storage are calculated on a grid cell basis while hydraulic processes of runoff, channel flow and shallow flooding are computed based on kinematic wave equation (1D) and Saint-Venant equations (2D) (Jetten, 2014).

Interception

The canopy cover interferes with the amount of rainfall that reaches the ground surface through process of interception. The model identifies the canopy as a water storage with limited capacity, hence, the amount the canopy can't store overflows into the ground surface (Jetten, n.d.). The amount of rainfall that the canopy intercepts is computed based on leaf area index and parameters set for different type of vegetation canopy.

Infiltration

Simulations performed in the study used the Green and Ampt infiltration equation to determine the potential infiltration rate of ground surface. This equation is based on Darcy's law, describing the downward flow of water through a soil medium. The equation is expressed as:

$$f = K_{sat} \cdot \left(\frac{(\Theta_s - \Theta_i) \cdot dh}{F} + 1 \right) \quad (4)$$

Where Θ_s = soil porosity
 Θ_i = initial soil moisture
 dH = suction at wetting front
 F = cumulative infiltration amount
 f = potential infiltration rate in mm/h

$$f_{actual} = \min(\text{rainfall intensity}, f) \quad (5)$$

The actual infiltration rate per timestep however, is determined from the minimum value between the rainfall intensity and potential infiltration rate, as seen in Equation 5. When potential infiltration rate is higher than rainfall intensity, rainfall amount falling at a given period is absorbed by the surface. When potential infiltration rate is lower than rainfall rate, not all rainfall is accommodated by the surface and this results to an infiltration excess overland flow.

When soil is fully saturated and initial soil moisture equals the soil porosity, the potential infiltration rate equals the saturated hydraulic conductivity. If the lower soil boundary is made impermeable, there is no infiltration process occurring in the catchment and all rainfall reaching the ground surface is converted to runoff. When the soil storage capacity is overcome by infiltrated water, additional water coming into the catchment is automatically converted to runoff.

Overland flow

Rainfall that reaches the ground surface but does not enter the substrate is converted to runoff. Runoff is routed to the outlet through the local drainage direction flow. When water height in the channel overcomes the channel depth, water is distributed over the flood zone using the DEM and Saint-Venant equations for shallow water flow. Shallow water flow refers to condition where the flow velocity is assumed uniform over a vertical profile.

3.4.1 Input requirements of LiSEM database

The single-event based operation of LiSEM requires high temporal resolution of rainfall input. In terms of catchment characteristics, LiSEM requires data characterizing topography, soil cover and land cover. Table 3.3 presents the main data that is required in LiSEM while Table 3.4 shows the parameter maps generated from the main group of input data.

The computation of LiSEM on a pixel by pixel basis requires that all inputs are of the same resolution, the same number of pixels and are perfectly stacked over each other. The resolution employed in preparing the LiSEM database is 30x30 meters. The digital elevation model (DEM) which was at 5m resolution was prepared by resampling the image to 30m using bilinear interpolation.

Type of data	Source	Remarks
Rainfall	Rainfall design event	Based on data from Thai Met Office
DEM	Land Development Department, Thailand	5x5 m resolution
Land use/land cover of 2000 and 2016	Asian Disaster Preparedness Center	30x30 m resolution
Vegetation cover	Satellite imagery	30x30 m resolution
Soil cover map	Soil unit map from Solomon, 2005	
Soil physical information	2017 fieldwork, pedotransfer functions based on Saxton, 2006	

Table 3.3 Main data required for constructing LiSEM database

Parameter	Name	Source
<u>Catchment</u>		
DEM	dem.map	DEM
Gradient	grad.map	DEM
Local drain direction	ldd.map	DEM
Outlet	outlet.map	DEM
<u>Landuse</u>		
Units	landunit.map	Land cover
Vegetation cover fraction	per.map	Vegetation cover
Vegetation height	ch.map	field observation
<u>Soil surface</u>		
Random roughness	rr.map	Literature-derived
Manning's coefficient	n.map	Literature-derived
<u>Green and Ampt Layer 1</u>		
Saturated hydraulic conductivity	ksat1.map	field measurement
Suction at wetting front	psi1.map	Literature-derived
Porosity	thetas1.map	field measurement
Initial soil moisture	thetai1.map	field measurement
Soil depth	soildepth.map	DEM
<u>Channels</u>		
Local drain direction of channels	lddchan.map	ldd.map
Channel gradient	changrad.map	grad.map
Channel Manning's	chanman.map	Literature-derived
Channel width	chanwidth.map	ldd.map

Table 3.4 Parameter requirements of LiSEM for hydrological simulations

3.4.2 Soil data for hydrologic simulation

Soil physical properties are influential in the infiltration process. The infiltration rate and storage capacity of soils determines the percent of rainfall converted to runoff. Aside from intrinsic soil property of porosity, the storage capacity is also determined by the soil depth.

An algorithm to predict soil depth based on distance to fluvial channel and gradient of steepness was developed by Kuriakose (2009) for Ghats Mountains in Kerala, India. The Ghats is dominated by a tropical climate and average annual rainfall is over 250 cm. The relative similarity between the climate and annual rainfall amount of the Ghats and the study area justifies the use of the soil depth algorithm for the Nam Chun catchment. The algorithm expresses soil depth as:

$$\text{Soil depth} = \text{Intersect} - a \cdot \text{DEM} - b \cdot \text{Channel Distance} - c \cdot \text{Gradient} - d \cdot \text{Curvature} \quad (6)$$

Where Intersect = 30.083

A = 0.00143

B = 0.00062

C = 2.6718

D = 2.746

The coefficients serve as normalizing parameters for the soil depth. Exposures observed along road cuts during fieldwork substantiate the veracity of derived soil thickness. The resulting soil depth map is shown in Figure 3.3.

Information about the soil texture classes present in the study area is available based on earlier work by Solomon (2005). Figure 3.4 shows the soil texture map of Namchun. Soil characteristics based on pedotransfer functions by Saxton & Rawls (2006) are presented in Table 3.5.

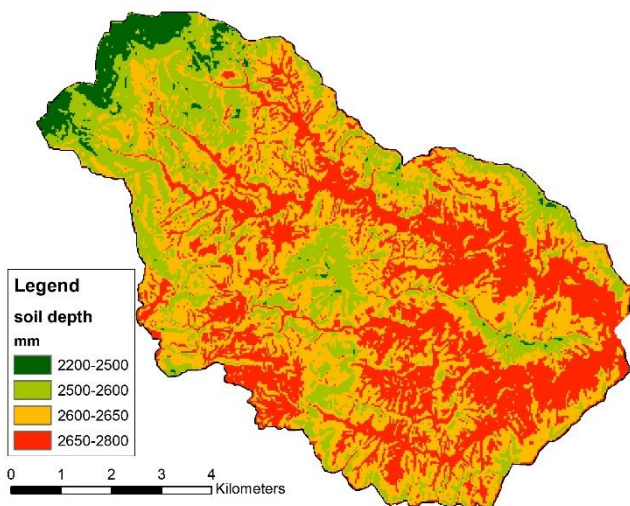


Figure 3.3 Soil depth map of study area

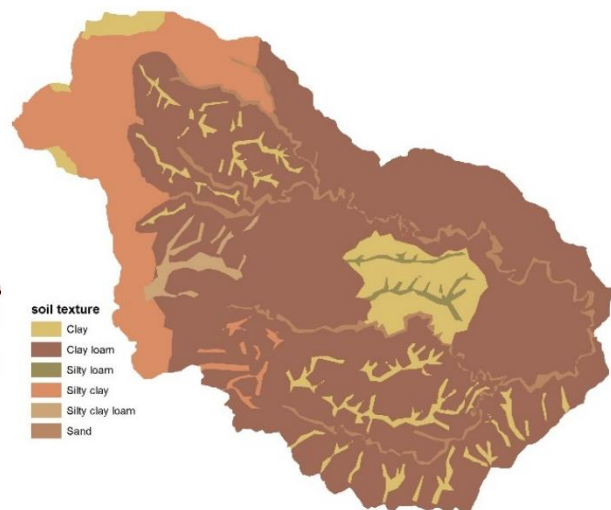


Figure 3.4 Map of soil texture classes in the study area

Soil texture	Field capacity (%)	Wilting point (%)	Porosity (%)	Suction at wetting front (cm)
Clay	45.4	34.2	51	31.6
Clay loam	36.0	23.6	51	20.9
Silty clay	39.7	25.3	56	29.2
Silty clay loam	38.7	23.1	57	27.3
Sandy loam	24.7	13.2	46	11.0

Table 3.5 Soil characteristics used as input in the simulation

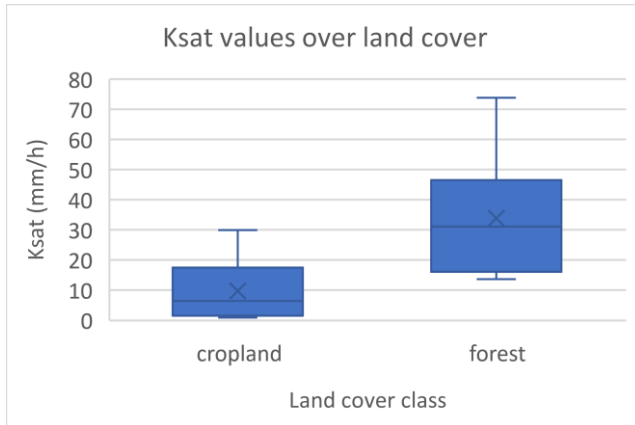


Figure 3.5 Box plot of ksats values with respect to dominant land cover classes

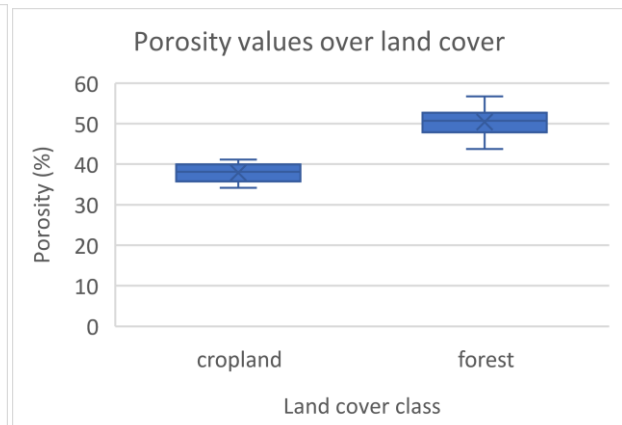


Figure 3.6 Box plot of porosity values with respect to dominant land cover classes

Values of saturated hydraulic conductivity of soil was obtained from samples collected from September 2017. Data were added to soil data already present from earlier works. The values of ksats and porosity were classified according to dominant land cover classes and the statistical summary of these values are presented in Table 3.6. The box plot of ksats and porosity over land cover classes are presented in Figure 3.5 and 3.6.

Results show that croplands have a mean ksats value of 9.7 mm/hour while forests have mean ksats value of 33.9 mm/h. Mean porosity in croplands is 38% and 50% in forest. Field data indicates that infiltration and moisture storage capacities are higher in forests compared to croplands.

	Ksat (mm/h)		Porosity (%)	
	cropland	forest	cropland	forest
Mean	9.7	33.9	37.9	50.4
Max	29.9	73.8	41.1	56.7
Min	0.86	13.7	34.2	43.7
n	11	12	5	15

Table 3.6 Statistical summary of ksats and porosity values obtained from the catchment

3.4.3 Calibration using discharge data

Sub daily discharge data is recorded for Namchun catchment during 1 July – 31 October 2005. The discharge is recorded on a three-hour interval for twelve hours in each day starting at 06:00 until 18:00. This causes a 12-hour gap between the last discharge measurement for a given day and the first discharge measurement of the next day. The discharge measurements were recorded when the reservoir was not yet constructed. In order to approximate the conditions during the discharge measurement, land cover from year 2000 was used in the calibration.

Because there is no sub daily rainfall record for Namchun, the daily rainfall recorded in Lom Sak is used to determine the rainfall input for model calibration. Based on the record, the maximum daily rainfall logged for 2005 was 75.7 mm which was recorded during September. The rainfall analysis in Section 3.2 identifies this daily rainfall amount as 2-yr return period rainfall event. The 2-yr return period design storm was used as rainfall input for calibrating the model and field capacity as initial soil moisture based on the type of season the discharge was measured. Maximum discharge value recorded during the period was 32000 l/s on 6 September; the measurement between 6:00 on 6 September to 6:00 7 September was used in model calibration.

3.4.4 Scenarios for simulation

To fulfill the objective on assessing how different initial soil moisture conditions can generate catchment response, several scenarios were conceived. The scenarios are based on the rainfall return period, land cover and initial soil moisture at field capacity, wilting point and complete saturation. The combination of different conditions are presented in Table 3.7.

Scenario	Initial soil moisture	Land cover	Rainfall RP
FC_2000_2YR	FC	2000	1:2
FC_2016_2YR	FC	2016	1:2
FC_2016_5YR	FC	2016	1:5
FC_2016_10YR	FC	2016	1:10
FC_2016-20YR	FC	2016	1:20
FC_2016_50YR	FC	2016	1:50
FS_2016_2YR	FS	2016	1:2
FS_2000_2YR	FS	2000	1:2
WP_2016_2YR	WP	2016	1:2
WP_2016_5YR	WP	2016	1:5
WP_2016_10YR	WP	2016	1:10
WP_2016_20YR	WP	2016	1:20
WP_2016_50YR	WP	2016	1:50

Table 3.7 Combination of different conditions of rainfall, land cover and initial soil moisture to create scenarios for simulation
FC = field capacity FS = full saturation WP = wilting point

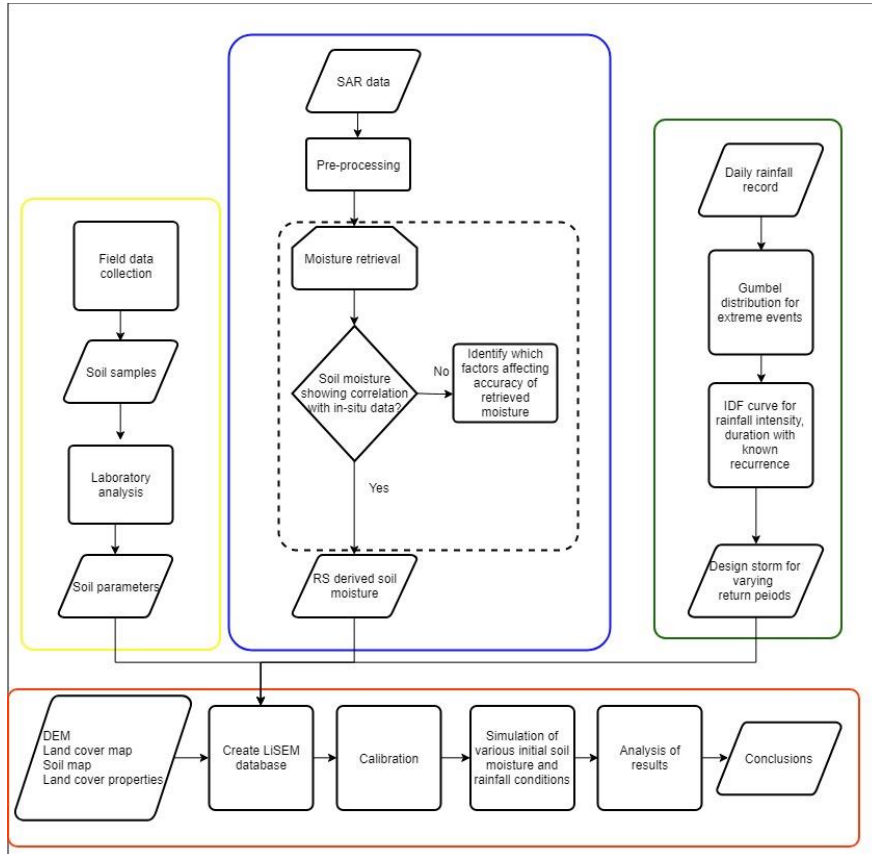


Figure 3.7 Flowchart diagram used in the study

4 SOIL MOISTURE MEASUREMENT AND RETRIEVAL FROM RADAR

4.1 Soil moisture based on in-situ data

Soil moisture measurement was collected from three primary land covers: forest, cropland and grasslands, in varying terrains and soil texture classes. Most of the soil moisture readings obtained in grasslands are located in the flat plains approximately 3km east outside Namchun catchment. Terrain is classified as flat, moderate and steep. Flat terrains are characterized by gradients less than 5 degrees, moderate terrains have gradients between 5-20 degrees and steep terrains have gradients between 21-40 degrees. Very steep terrain are characterized as having greater than 40 degrees slope gradients, however, it must be noted that measurements were not obtained from such terrains.

4.1.1 Soil moisture variability and topography

The ruggedness of the study area constrains well-distributed sampling strategy. Location of in-situ measurements are presented in Figure 4.1 as well as the slope map of the study area and statistics of soil moisture measured per slope gradient is presented in Table 4.1

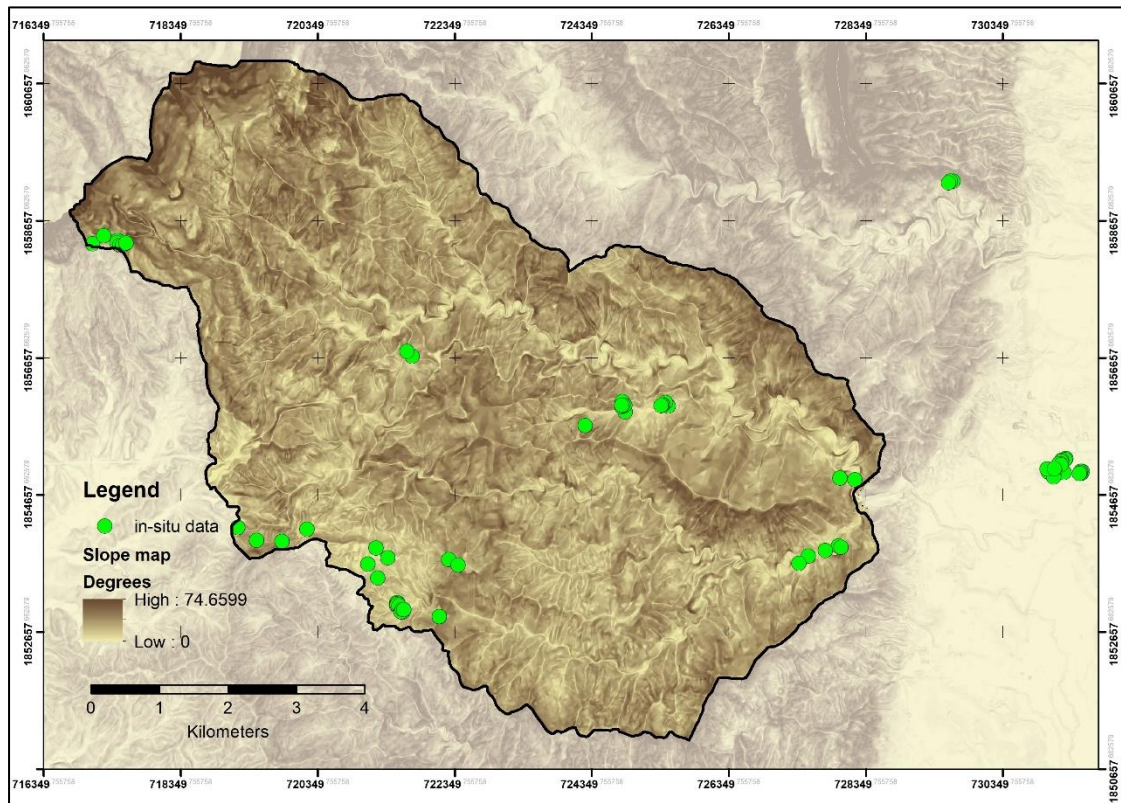


Figure 4.1 Location of soil moisture measurements obtained during the field work

Based on field measurements mean soil moisture increases as steepness increases from 0.294 in flat areas to 0.393 in steep areas. Meanwhile the standard deviation increases with decreasing steepness from 0.046 in steep areas to 0.117 in flat areas.

This observed relationship in the study area is contrary to that reported by Hawley, et al., (1983) where soil moisture values are higher at flat areas compared to the top of the slope given a minor catchment with limited topographic differences. Charpentier & Groffman (1992) has also reported the lower variability of soil moisture values in flat lands compared to that of sloping terrains. However, Western, et al. (2003) noted

that terrain characteristic is a poor indicator of soil moisture variability and underscores that soil properties and annual seasonal climate conditions have stronger impact on the pattern and variability of soil moisture.

	Slope gradient classification		
	Flat (0-5)	Moderate (5-20)	Steep (>20)
Mean (m ³ /m ³)	0.29	0.39	0.39
Min (m ³ /m ³)	0.12	0.22	0.31
Max (m ³ /m ³)	0.51	0.51	0.47
Stdev	0.12	0.07	0.05
<i>n</i>	22	35	14

Table 4.1 Statistics of soil moisture values obtained from different slope gradients in the study area

4.1.2. Soil moisture variability and vegetation

The results of field measurements of soil moisture show varying mean soil moisture values with respect to different land covers is shown in Table 4.2. Data shows that lowest mean soil moisture is present in grasslands and highest in croplands, varying from 0.27 to 0.41 while forest has mean value at 0.36. The standard deviation of soil moisture values across land covers show that grasslands have the highest variation of soil moisture at 0.11 and croplands the lowest at 0.06 while forest is at the middle with 0.08.

The land cover adapted here is classified primarily on the type and density of vegetation present. Vegetation affects soil moisture due to its water uptake in the root zone as well as its role in rainfall interception by limiting direct rainfall impact onto the ground surface. In the case of Namchun, croplands and forest show higher soil moisture values compared to grassland. This observation is opposite that of Garcia-Estringana, et al. (2012) where in a catchment, grasslands located at downslope terraces show higher soil moisture compared to canopy-covered sampling points. The lower variability of soil moisture in areas with greater vegetation canopy corroborates the findings of Mohanty & Skaggs (2001), according to which, fuller canopy covers show lower variability compared to soil moisture measured in areas with lesser canopy coverage.

	Land use units		
	Grassland	Cropland	Forest
Mean (m ³ /m ³)	0.27	0.41	0.36
Min (m ³ /m ³)	0.12	0.22	0.19
Max (m ³ /m ³)	0.48	0.51	0.51
Stdev	0.11	0.07	0.08
<i>n</i>	15	32	24

Table 4.2 Statistics of soil moisture values obtained from different land cover units in the study area

4.1.3 Soil moisture variability and soil texture

Classifying in-situ soil moisture with respect to soil texture shows that clay loam has the highest mean soil moisture value at 0.41, followed by sandy loam at 0.33, silty clay at 0.37. Meanwhile the standard deviation shows that highest variation is present in sandy loam at 0.124 and lowest in sandy loam at 0.07. Table 4.3 shows the summary of soil moisture values over soil texture class. Mean soil moisture obtained for each soil texture class shows higher soil moisture for textures with higher clay content.

	Soil texture class		
	Clay loam	Sandy loam	Silty clay
Mean (m ³ /m ³)	0.41	0.33	0.37
Min (m ³ /m ³)	0.19	0.12	0.27
Max (m ³ /m ³)	0.51	0.51	0.51
Stdev	0.07	0.11	0.07
<i>n</i>	21	30	13

Figure 4.3 Statistics of soil moisture obtained from different soil texture classes in the study area

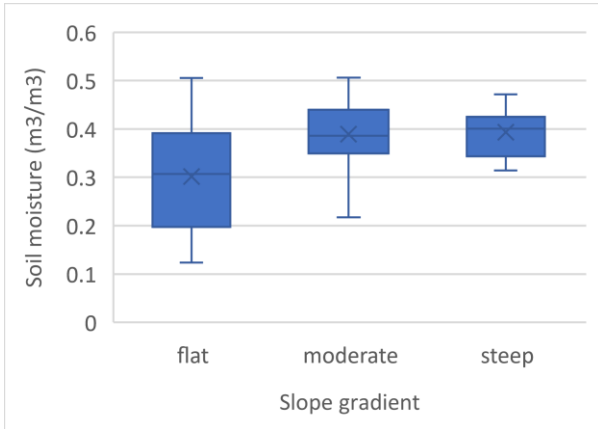


Figure 4.2 Box plot of soil moisture values over slope gradient

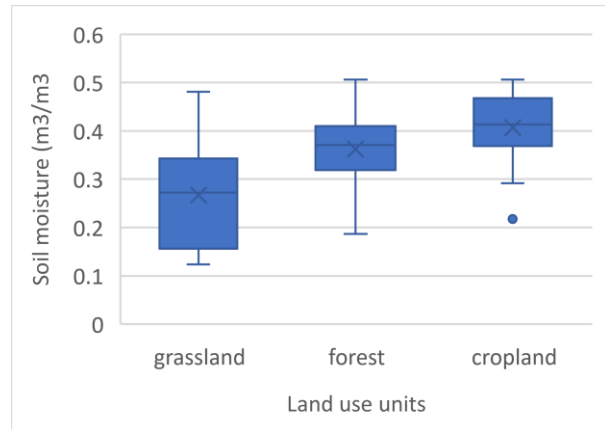


Figure 4.3 Box plot of soil moisture values and land use units

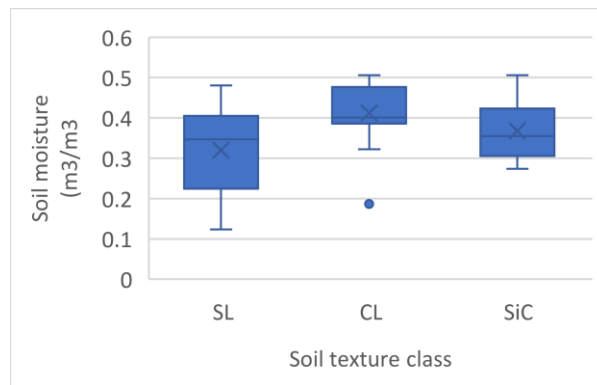


Figure 4.4 Box plot of soil moisture and soil texture class

Land cover	Soil texture	Gradient	Soil moisture value	Standard deviation
Grassland	Sandy loam	Flat	0.28	0.12
Forest	Silty clay	Moderate	0.33	0.04
Forest	Clay loam	Flat	0.35	-
Cropland	Sandy loam	Flat	0.37	-
Cropland	Sandy loam	Moderate	0.38	-
Cropland	Silty clay	Moderate	0.38	-
Forest	Sandy loam	Moderate	0.39	-
Forest	Silty clay	Steep	0.4	0.05
Cropland	Sandy loam	Steep	0.4	0.03
Forest	Clay loam	Moderate	0.42	0.05
Cropland	Clay loam	Flat	0.42	-
Cropland	Clay loam	Moderate	0.44	0.04
Cropland	Clay loam	Steep	0.47	-

Table 4.4 Mean soil moisture values derived from Boolean combinations of land cover, soil texture and gradient

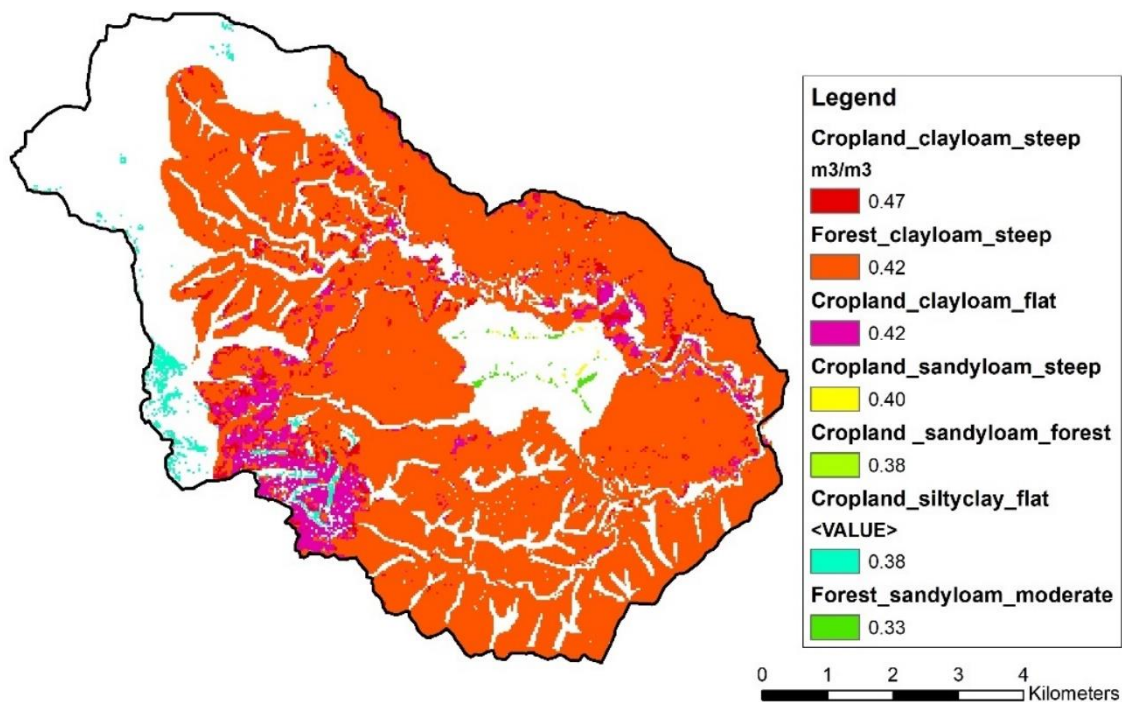


Figure 4.5 Soil moisture map based on Boolean operation of catchment characteristics and average in-situ soil moisture value of the elements

Box plots from Figures 4.2, 4.3, and 4.4 show the variation of soil moisture over slope gradient, soil texture class and land use units. Based on the plots, soil moisture clusters more distinctly over land use units, lending distinct soil moisture mean value for land use units. The mean soil moisture values in soil texture class show slight increase in value for textures with higher clay content.

Boolean operation was used in grouping the soil moisture classes as presented in Table 4.4. Soil moisture class is based on land use, soil texture and gradient. The soil moisture value was obtained by averaging the soil moisture of the elements within the class. This assumes that areas with similar land cover, gradients and soil texture will have the same soil moisture value. Applying the values of the soil moisture class produces a soil moisture map, presented in Figure 4.5 The resulting soil moisture map shows a uniform soil moisture value for large parts of the catchment.

Soil moisture map generated using this method shows the small variation of soil moisture values in the study area. This is likely an effect of soil moisture sampling during the wet conditions where soil moisture values are in their higher range.

4.2 Soil wetness based on radar remote sensing

4.2.1. Results of change detection method

The method of change detection applied in retrieval of soil moisture required multiple radar images from which the mean radar backscatter and standard deviation of radar backscatter per pixel position are retrieved. The method uses the mean and standard deviation to obtain wet and dry reference image. By determining a dry reference image with minimal soil moisture, the backscatter of roughness and vegetation could be represented in a single image.

This dry reference image is obtained using the mean radar backscatter and standard deviation of all radar images retrieved from October 2016 – September 2017. 63 radar images were retrieved from the entire period. Radar images were acquired by the satellite at approximately 5 day intervals. The resulting mean per pixel and standard deviation per pixel is presented in Figure 4.6. The mean backscatter image represents the mean values for the pixel location derived from all the elements of the radar image stack. The standard deviation backscatter image represents the dispersion of backscatter values from mean backscatter.

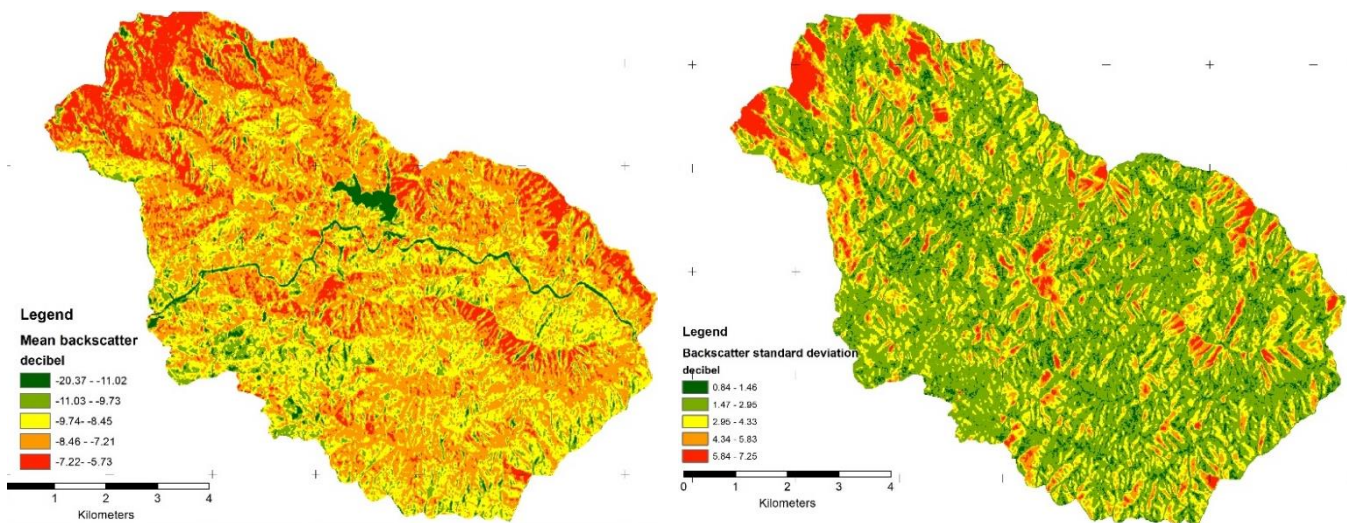


Figure 4.6 Mean backscatter and standard deviation of radar backscatter obtained during October 2016-September 2017 period

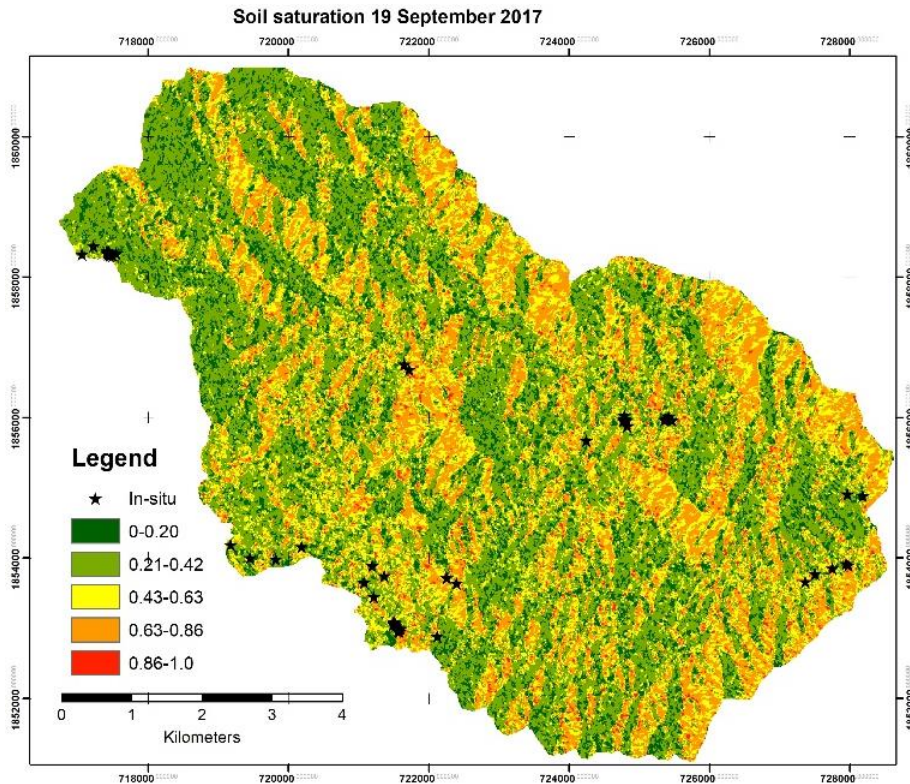


Figure 4.7 Derived soil saturation conditions during 19 September 2017

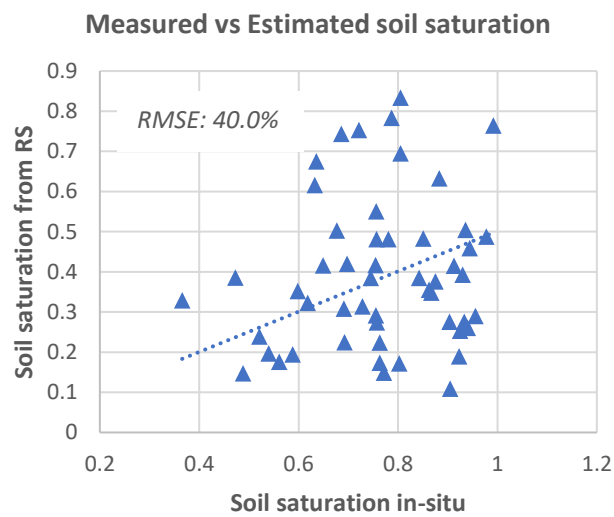


Figure 4.8 Comparison of measured soil saturation based on field data with estimated soil saturation based on values retrieved from change detection.

The results of applying the change detection method on 19 September radar image is presented in Figure 4.7 and the correlation of retrieved soil moisture is compared with in-situ values as shown in Figure 4.8. The measured soil moisture data was converted to soil saturation by dividing the values by the soil porosity. The root mean square error between the measured values and estimated values is at 40%. The validation of change detection method shows that majority of the remotely sensed soil saturation is underestimated in comparison to the measured values.

The resulting soil saturation map from September 19 acquisition shows a pattern of high saturation values in the southwest facing slopes. The mean backscatter and standard deviation backscatter images also show high values in the same south-west facing slopes.

4.2.2 Catchment influence on radar backscatter

Backscatter intensity received by a radar sensor is affected by terrain conditions. Because it is a side-looking instrument, radar sends out energy pulses at an incidence angle with respect to the normal earth vector. Foreshortening occurs when slopes facing the radar are compressed in the image captured which causes enhanced backscatter values (ESA, 2007). The trend of increase in radar backscatter with respect to slope gradient is presented in Figure 4.9 where standard deviation of backscatter values is higher in steep slopes. The radar wavelength at C Band (5.4 cm) is intercepted by canopy leaves and trunks. The backscatter reading that is detected by the sensor in dense vegetation will carry higher signals of dielectric property of leaves and trunk and lesser signal from soil surface (Moran, 2004).

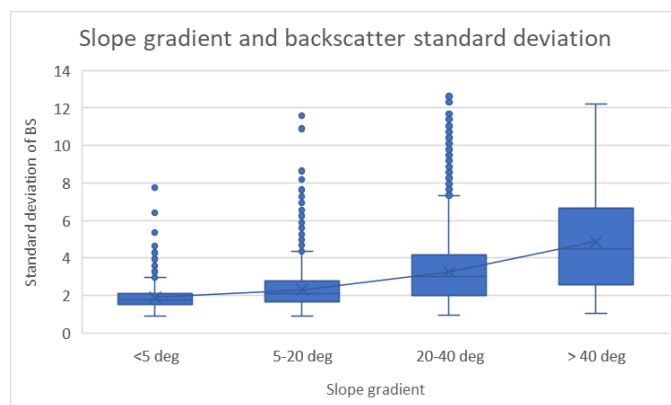


Figure 4.9 Box plot of slope gradient and backscatter standard deviation

The high spatial resolution acquisition of Sentinel is useful for catchment modelling at Namchun, however, the rugged terrain of the study area limits the accuracy of radar backscatter. This effect reduces the accuracy of retrieved soil moisture. Although the radar data was corrected for terrain displacement, the correction is not sufficient to eliminate effects of foreshortening, Because of the low accuracy of remotely-sensed soil moisture, it could not be used in initialization conditions for the event-based simulation of the rainfall-runoff in the Namchun catchment.

5. LISEM SIMULATIONS

This section presents the results of LiSEM simulations with different combinations of initial soil moisture, rainfall characteristic and land cover. The combinations of which were described in Table 3.6. The first section of the chapter discusses the result of model calibration while the succeeding section discusses the simulation scenarios. The last part of the chapter concerns the simulation of a previous disaster event in the study area.

5.1 Results of model calibration

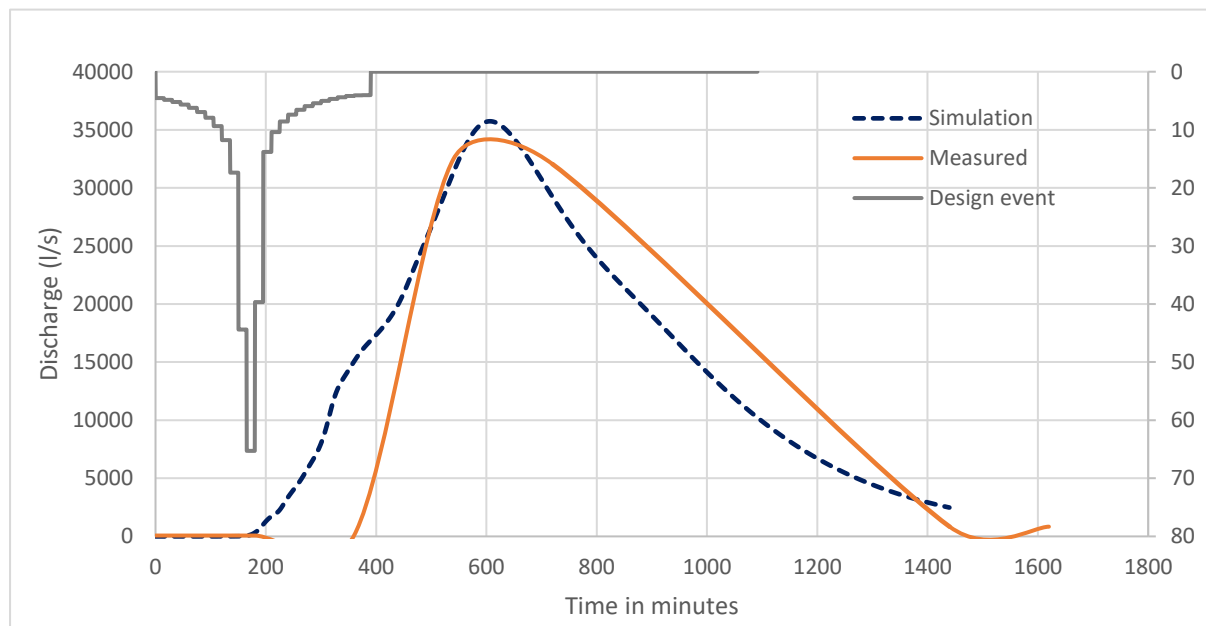


Figure 5.1 Hydrograph of measured discharge and used in calibration and resulting simulated values

The model was calibrated from an enhanced discharged event recorded in September 2005 and using the design rainfall event with a 2-year return period. The maximum daily rainfall obtained for 2005 is 75.7 mm during the month of September. Rainfall analysis in Chapter 3 classifies this maximum daily amount as 1:2 year event. Because there is no subdaily precipitation data accompanying the discharge data, a design rainfall event was used as input that could have caused the measured values. The measured discharge was obtained during the rainy season, thus, the initial soil moisture used is at field capacity. Land cover from 2000 was also used to better represent land use units corresponding to 2005 scenario, when artificial reservoir was not yet present. Total volume of measured discharge is 708,049,080 m³ while its peak is discharge is at 32,459 l/s with a response time of 465 minutes. Figure 5.1 shows the hydrograph of measured and simulated values and Table 5.1 gives its summary. Using the Ksat for slopes, the peak discharge for a high intensity rainfall was calibrated to 34,832 l/s while the response time was calibrated to 437 minutes using Manning's number for channels. Factors used for calibration are provided in Table 5.2.

	Measured			Simulated		
	Total volume (m ³)	Peak discharge (l/s)	Response time (minutes)	Total volume (m ³)	Peak discharge (l/s)	Response time (minutes)
2-yr event	708,049,080	32,459	465	1,171,248	34,833	437

Table 5.1 Measured data used for calibration and simulated results after calibration for a 2-yr event rainfall

Event	Calibration parameters			
	Ksat (slopes)	Ksat (channel)	Manning's (channel)	Manning's (slopes)
High intensity	0.45	1	1.5	1

Table 5.2 Calibration factors used in simulation

The simulated discharge shows an overestimation of total discharge volume in the catchment, however, peak discharge and response time was able to approximate the measured values. The discrepancy in the total discharge volume and general shape of the discharge graph may come from the rainfall situation in the actual measurement. The rainfall that induced the measured discharge may not be uniform throughout the whole catchment, hence the steep ascent to peak discharge and its gradual decrease. Meanwhile, the simulation assumes that the catchment is receiving uniform amount of rainfall per unit of time.

Sub-catchments within Namchun

Two sub-catchments inside Namchun are identified to examine the runoff discharge. Outlet 1 is located at the current reservoir inlet and Outlet 2 is located at the southern part of Namchun. Figure 5.2 shows the location of the outlet points and the size sub-catchment that it drains. Outlet 1 drains approximately 20 km² of land area and Outlet 2 drains 25 km² of land area. The 2016 land cover map in Figure 5.3 shows that forest is the main land cover of the upstream area of Outlet 1. Outlet 2 drains a sub-catchment that has mixed land cover. Land cover map of 2016 shows that croplands are concentrated in the most upstream areas of Outlet 2. The shape

5.2 Catchment response to change in land cover

Assessment of land cover maps from Figure 5.3 and 5.4 shows the significant change in the land cover in the area from 2000 to 2016. A summary matrix of land cover change is presented in Table 5.3. Columns represent the land cover class from year 2000 while the rows represent the change of a land cover class to another.

Forest land cover which is 4,540 hectares in 2000 has increased in land area to 5,750 hectares in 2016. The biggest source of land area that contributed to increase of forest is cropland. 1,250 hectares of cropland, equivalent to 72% of total cropland area of 2000 was converted to forest. 258 hectares of grassland areas in 2000 was also converted to forest. The increase of forest land from 2000 – 2016 is motivated by local policies of the Land Development Department (personal communication with LDD employee, September 2017). Figure 5.5 shows the location of croplands and grasslands in 2000 that have been converted to forest cover by 2016.

		2000 Land cover					GAIN
		grassland	builtup	cropland	forest	Total area (ha)	
2016 Land cover	grassland	2.97		8.82	8.73	20.52	17.55
	builtup	2.16	2.7	25.11	48.69	78.66	75.96
	cropland	71.73	2.52	452.16	209.52	735.93	283.77
	forest	258.12	4.05	1248.21	4253.58	5763.96	1510.38
	water	1.62			15.84	17.46	
	Total area (ha)	336.6	9.27	1734.3	4536.36	6616.53	
	LOSS	333.63	6.57	1282.14	282.78		

Table 5.3 Summary matrix of land cover change of Namchun from 2000 to 2016

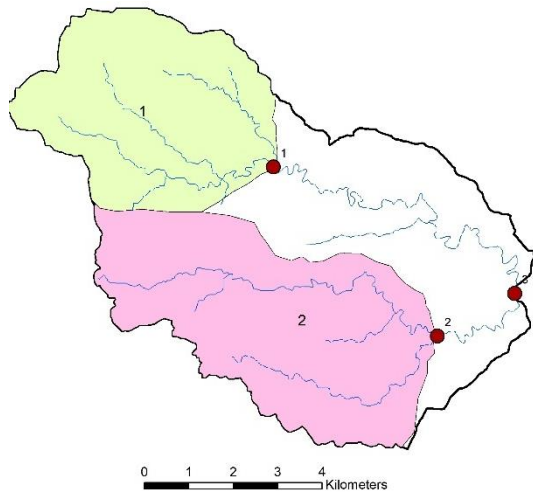


Figure 5.2 Sub-catchments within Namchun

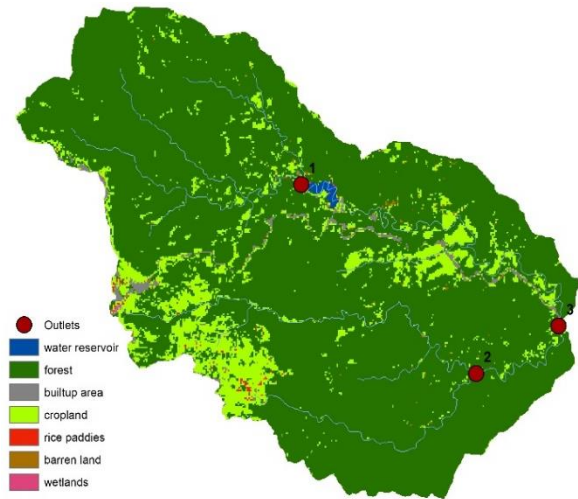


Figure 5.3 2016 land cover



Figure 5.4 2000 land cover

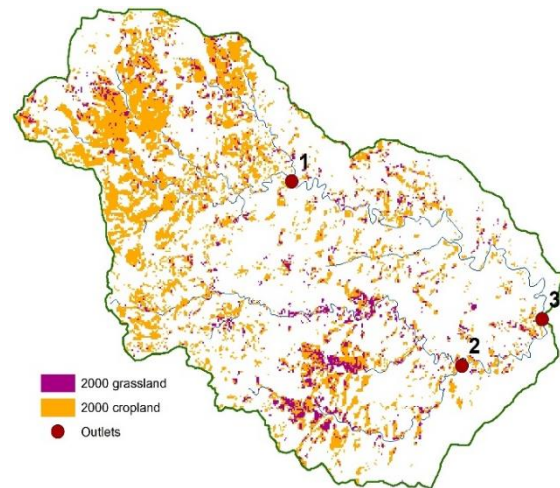


Figure 5.5 Grassland and cropland converted to forest

The response of the catchment to change in land cover is assessed through hydrologic simulation. Land cover from 2000 and from 2016 was used in the simulation. The response of the catchment to a rainfall event is examined at Outlets 1 & 2.

The result of catchment response due to land cover change in sub-catchment of Outlet 1 is presented in Figure 5.6. The hydrograph shows the catchment response at Outlet 1 with decreasing peak discharge from 16,900 l/s in 2000 to 6,200 l/s in 2016. The lag time increased by 75 minutes from 225 minutes in 2000 to 290 minutes in 2016. Discharge volume decreased by 123 000 m³.

The same scenario is observed in Outlet 2, with hydrograph presented in Figure 5.4, when discharge from 2000 simulation decreased from 14,000 l/s to 8,100 l/s in 2016. There is a significant increase in response time from 320 minutes to 618 minutes. Total discharge volume also decreased from 416,800 m³ in 2000 to 374,800 m³ in 2016. Table 5.4 provides a summary of catchment response due to land cover change from 2000-2016.

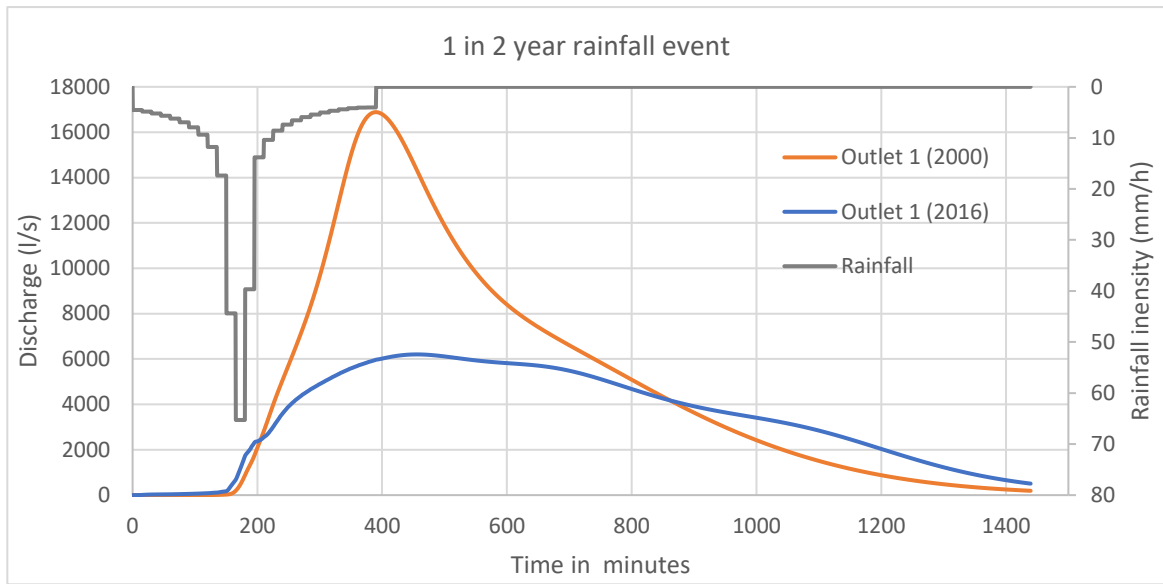


Figure 5.6 Catchment response at Outlet 1 with different land covers and initial soil moisture at FC

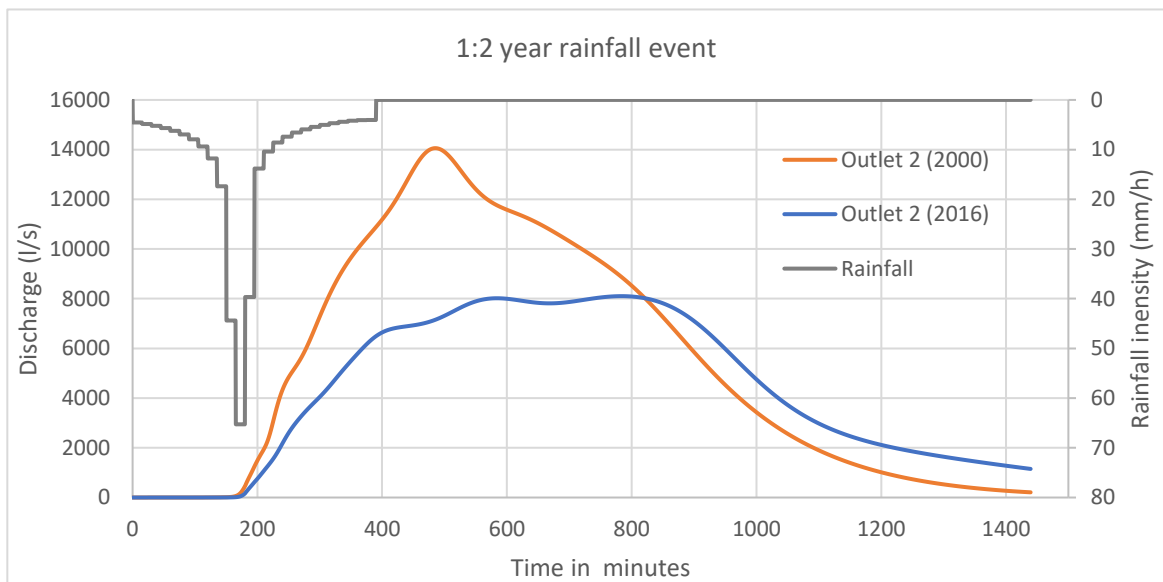


Figure 5.7 Catchment response at Outlet 2 with different land covers and initial soil moisture at FC

Assessment of land cover in the upstream part of Outlet 1 shows drastic change from dominantly cropland area to forest. The change in catchment response can be attributed to the effect of land cover in the hydraulic property of soils (Perkins, et al., 2012). The conversion of croplands to forest land changes the soil hydraulic property of the land unit through decrease of surface compaction and tilling. The change in land cover not only changes the amount of runoff but also the response time to the rainfall event. Converting units into forest land has caused an increase in the time delay between the maximum rainfall intensity and peak runoff discharge.

The 2016 hydrograph in Outlet 2 in Figure 5.7 also shows distinct changes from its 2000 counterpart. The change in land cover units from predominantly cropland to forest land contributed to the higher infiltration in the sub-catchment. Overland flow is also taking longer time to reach the channels

Rainfall return period	1 in 2	1 in 2
Land cover	LC 2000	LC 2016
Initial soil moisture	FC	FC
Precipitation (mm)	78.4	78.4
Runoff (mm)	17.7	14.4
Interception (mm)	0.7	2.0
Infiltration (mm)	59.4	61.0
Peak Outlet 1 (l/s)	16,880	6,203
Peak Outlet 2 (l/s)	14,060	8,103
Peak time P (min)	165.5	165.5
Peak time Outlet 1 (min)	390	455.5
Peak time Outlet 2 (min)	485	783.5
Runoff coefficient (%)	22.6	18.4

Table 5.4 Summary of change in catchment response between 2000 land cover and 2016 land cover

The comparison of the catchment response from 2000 with 2-year rainfall event to land cover at 2016 with different rainfall return periods is shown in Figure 5.8. The peak discharge from 2000 land cover for a rainfall return period of 2 years is 17,000 l/s. The land cover of 2016 produces a similar peak discharge given a 20 year rainfall event. Peak discharge of this response is 18,000 l/s. Table 5.5 shows the values of peak discharge, peak time and discharge volume of response at 2-year rainfall and 20-year rainfall.

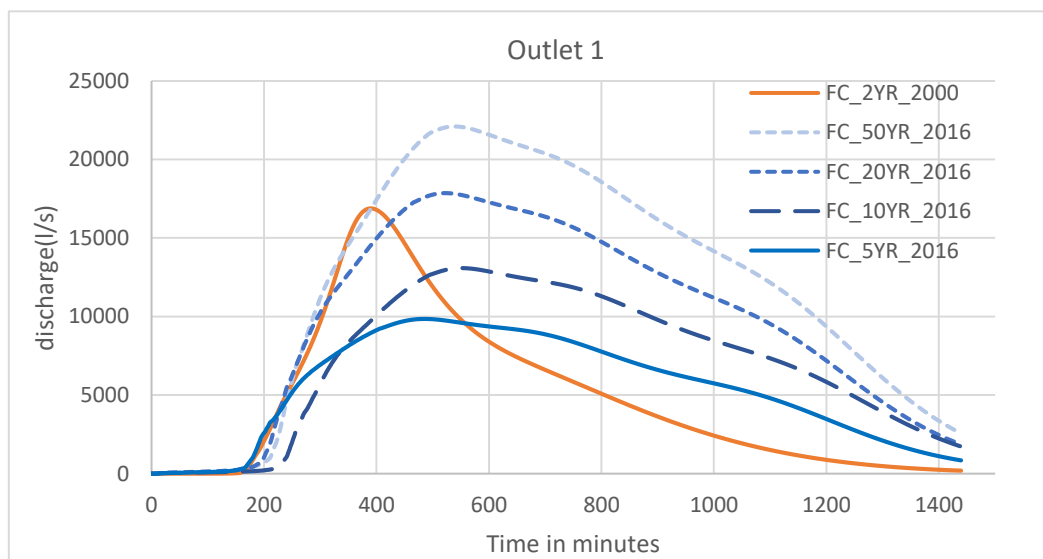


Figure 5.8 Catchment response at Outlet 1 for different rainfall events and land cover with same initial soil moisture

Scenario	FC_2YR_2000	FC_20YR_2016
Peak discharge (l/s)	16,884	17,856
Peak time (min)	390.0	523
Discharge volume (m ³)	295,350	843,565

Table 5.5 Comparison of peak discharge time between a 2 year rainfall event with 2000 land cover and 20 year rainfall event with 2016 land cover

5.3 Catchment response to various initial soil moisture conditions

LiSEM results for 2-year rainfall event with 2016 land cover			
Initial soil moisture	Wilting point	Field capacity	Full saturation
Runoff (mm)	8.7	14.4	72.1
Infiltration (mm)	66.9	61.0	-
Peak O1 (l/s)	3,670	6,200	36,530
Peak O2 (l/s)	5,220	8,100	38,890
Peak time P (min)	165.5	165.5	165.5
Peak time O1 (min)	352.0	455.5	536.0
Peak time O2 (min)	821.0	783.5	592.0
Response time O1 (min)	186.5	290.0	370.5
Response time O2 (min)	655.5	618.0	426.5
Runoff coefficient (%)	11.1	18.4	92.0

Table 5.6 Results of simulation on different initial soil moisture conditions with same rainfall return period and land cover

The results of LiSEM simulations for rainfall events with 2-year return periods of different initial soil moistures are presented in Table 5.6. The simulation shows an increasing discharge amount with increasing initial soil moisture conditions. There is also a rise in the peak discharge of both sub-catchments from 3,670 l/s in Outlet 1 for initial soil moisture at wilting point to 36,340 l/s when soil porosity is completely filled. Peak discharge at Outlet 2 increases from 5,215 l/s when initial soil moisture is at wilting point to 38,891 l/s at fully saturated conditions. The response time in Outlet 1 also reflects an increasing value with respect to increasing soil moisture. For Outlet 2 however, the response time decreases with increasing soil moisture.

Figure 5.9 is the hydrograph at Outlet 1 for high intensity 1:2 rainfall event. The hydrograph illustrates the nonlinear increase of runoff discharge volume when soil moisture equals the maximum storage capacity of the soil. Based on Green and Ampt infiltration equation, presented in Equation 4, when unsaturated depth equals zero, the infiltration rate is equal to the saturated hydraulic conductivity. In the case of simulation for the Namchun catchment, the lower soil boundary is rendered impermeable and infiltration amount is zero when soil is fully saturated.

The complete saturation of soil layer leads to almost tenfold increase in peak discharge at Outlet 1 compared to the peak discharge at field capacity conditions. This reflects the available storage capacity of the soil. Soil depth in Namchun, based on soil depth formula in Chapter 3 is 2200-2800mm. A 50% porosity, which is the porosity in most areas of the catchment, means available voids within a soil profile is 1100-1400mm. Given a 36% field capacity, the remaining unsaturated depth for a 2800 mm profile is 900mm.

The assumption that soil is fully saturated means that all available soil storage is filled. Because there is only one layer of soil considered, only first layer Green and Ampt is used in the model. This setup assumes that soil porosity is uniform over the entire soil profile and does not change with increasing depth. This assumption can lead to overestimation of soil storage capacity.

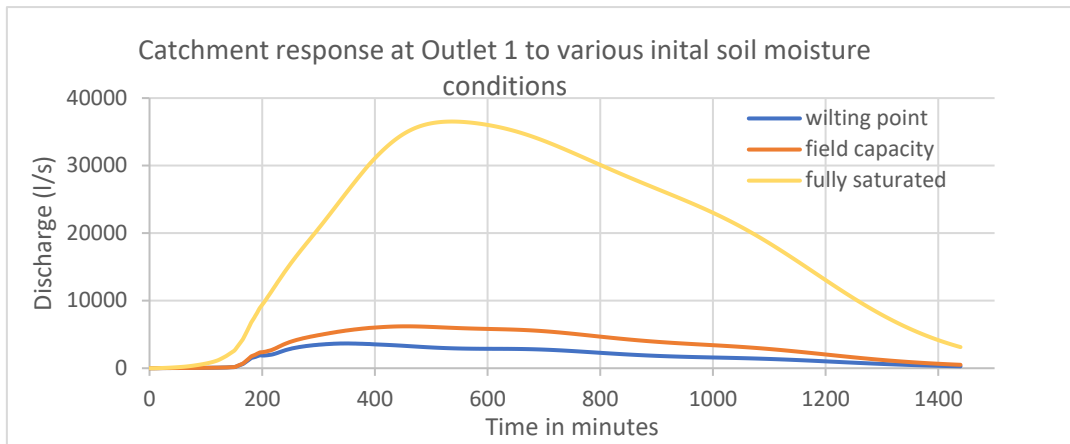


Figure 5.9 Hydrographs at Outlet 1 showing catchment response to 1:2 year rainfall with respect to various initial soil moisture

5.4 Similar catchment response to different rainfall event and soil moisture conditions

Results of simulation show that the catchment can behave similarly in its response to different rainfall return periods, given different initial soil moisture. The simulation of a 10 year rainfall event combined with wilting point soil moisture initial condition and that of a 5 year rainfall event that is initialized with wet soil moisture condition is summarized in Table 5.7. The resulting hydrographs from both simulations are shown in Figure 5.10 where the response between the two scenarios is similar.

Rainfall return period	1 in 5	1 in 10
Land cover	LC2016	LC 2016
Initial soil moisture	FC	WP
Precipitation (mm)	105.4	128.4
Runoff (mm)	22.0	21.5
Infiltration (mm)	79.9	102.9
Peak O1 (l/s)	9,850	9,467
Peak O2 (l/s)	12,170	12,815
Peak time P (min)	180.5	240.5
Peak time O1 (min)	485.5	518.5
Peak time O2 (min)	791.5	865.5
Response time O1 (min)	305	278
Response time O2 (min)	611	625
Runoff coefficient (%)	20.9	16.8

Table 5.7 Summary of catchment response to 10YRWP and 5YR FC scenario

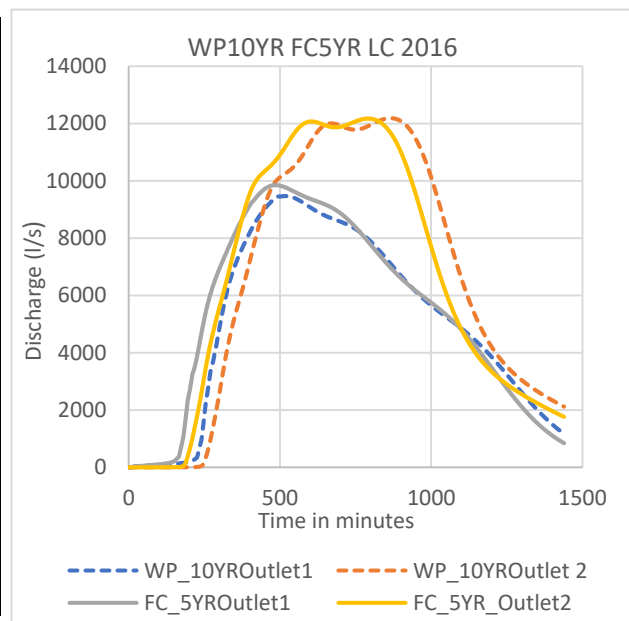


Figure 5.10 Simulation hydrographs of 10YR WP and 5YR FC

Another set of scenarios producing a similar catchment response is 20 year rainfall event with initial soil moisture at wilting point and a 10 year rainfall event with initial soil moisture at field capacity. Highest peak discharge from the combination of scenarios is at 17,065 l/s in Outlet 2 during wilting points conditions and 20 year rainfall. The summary of catchment response between the two scenarios are presented in Table 5.8. The resulting hydrograph of both simulations are presented in Figure 5.11.

Rainfall return period	1 in 10	1 in 20
Land cover	LC 2016	LC 2016
Initial soil moisture	FC	WP
Precipitation (mm)	128.4	148
Runoff (mm)	28.3	31.0
Infiltration (mm)	95.6	112.5
Peak O1 (l/s)	13,080	13,957
Peak O2 (l/s)	15,782	17,065
Peak time P (min)	240.5	211
Peak time O1 (min)	551.5	506
Peak time O2 (min)	846.5	819
Response time O1 (min)	311	295
Response time O2 (min)	606	608
Runoff coefficient (%)	22.1	20.9

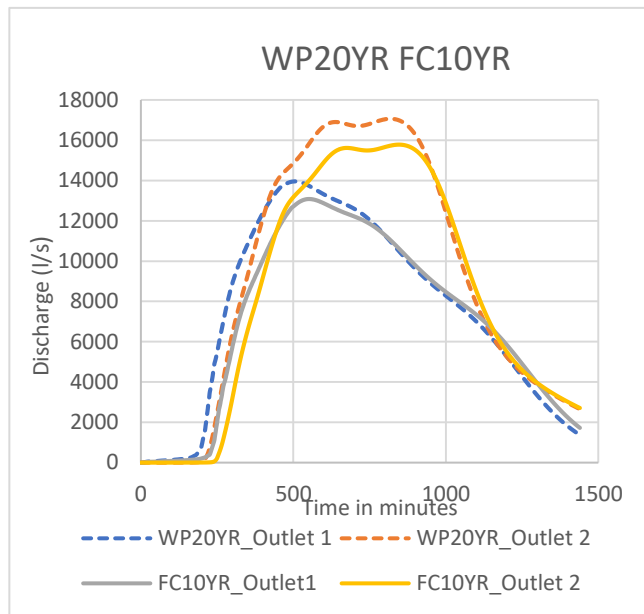


Table 5.8 Summary of catchment response to 20YRWP and 10YRFC

Figure 5.11 Hydrograph of catchment response of 20YRWP and 10YRFC

Rainfall return period	1 in 20	1 in 50
Land cover	LC 2016	LC 2016
Initial soil moisture	FC	WP
Precipitation (mm)	148	168
Runoff (mm)	38.6	38.9
Infiltration (mm)	104	124.4
Peak O1 (l/s)	17,856	17,781
Peak O2 (l/s)	21,154	21,328
Peak time P (min)	211	226
Peak time O1 (min)	523	525
Peak time O2 (min)	804	826
Response time O1 (min)	312	437
Response time O2 (min)	593	600
Runoff coefficient (%)	26.1	23.2

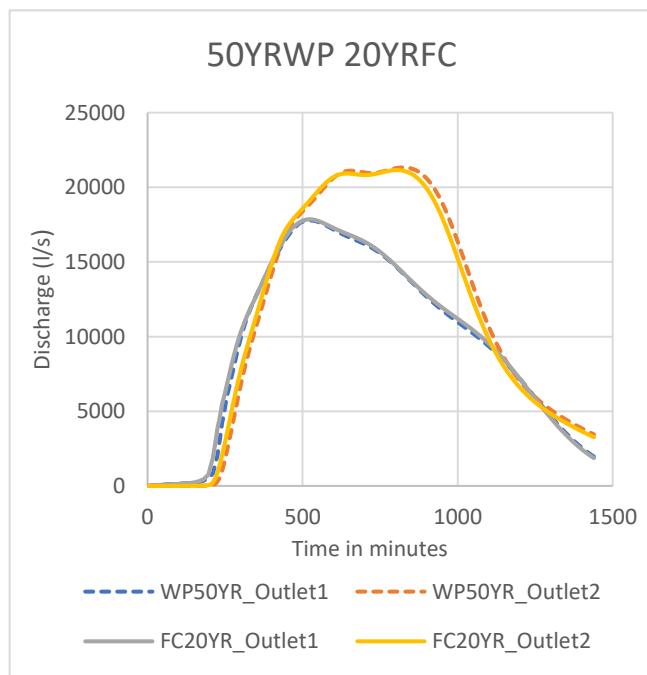


Table 5.9 Summary of catchment response to 50YRWP and 20YRFC

Figure 5.12 Hydrograph of catchment response of 50YRWP and 20YRFC

Another set of scenarios simulated are a 50 year rainfall event with initial soil moisture at wilting point and 20 year rainfall event at field capacity. Results show that the highest peak discharge from the set conditions is 21,300 l/s. The highest peak discharge is recorded in Outlet 2 and triggered by the 50yr rainfall event. The summary of catchment response is presented at Table 5.9 and the hydrographs in Figure 5.12.

The similar response of the catchment to different rainfall events is due to the amount of soil moisture present in the soil before the addition of rainfall into the system. Based on Equation 4, higher values of unsaturated depth contribute to higher amount of soil infiltration potential. Soil condition at wilting point has higher infiltration potential compared to soil condition at field capacity.

5.5 Simulation of previous hazard event

The 11 August 2001 hazard event in the study area has caused significant damage in Nam KoYai village that is located downstream of the discharge source. Records show that there were 9 days of rainfall prior to the event with accumulated rainfall amount of 104 mm.

Rainfall recorded in Lom Sak weather station on 11 August was 36 mm while maximum daily rainfall recorded during 2001 is 62 mm. Based on Gumbel distribution in Chapter 3.3, 62 mm rainfall amount has recurrence interval of 1.5 years. A rough simulation of the hazard event scenario is based on the 2000 land cover, 2-year rainfall event and fully saturated soil moisture condition.

Results of the simulation shows peak discharge in Outlet 1 at 54,400 l/s and 51,000 l/s in Outlet and a response time of 414 minutes and 496 minutes were recorded, respectively for both outlets. Discharge volume from Outlet 1 is 1.8 million m³ and 1.85 million m³ at Outlet 2. The summary of catchment response at hazard event is presented in Table 5.10 as well as the comparison of hazard event to other catchment responses.

Rainfall return period	1 in 2	1 in 50
Land cover	LC 2000	LC 2000
Initial soil moisture	FS	FC
Precipitation (mm)	78.4	168
Runoff (mm)	75.5	56.7
Interception (mm)	0.7	0.7
Infiltration (mm)	0	108.9
Peak O1 (l/s)	54,400	49,130
Peak O2 (l/s)	50,990	41,40
Peak O3 (l/s)	130,890	106,382
Total volume O1 (m ³)	1,787,990	1,370,000
Total volume O2 (m ³)	1,854,100	1,454,100
Total volume O3 (m ³)	4,984,450	3,760,860
Peak time P (min)	165.5	225.5
Peak time O1 (min)	414	463.5
Peak time O2 (min)	496	550.5
Peak time O3 (min)	604	661.5
Response time O1 (min)	248.5	238
Response time O2 (min)	330.5	325
Response time O3 (min)	438.5	436
Runoff coefficient (%)	96.3	33.8

Figure 5.10 Summary of catchment response to a 2-year rainfall event with fully saturated conditions and land cover in 2000

The response of the catchment to the fully saturated conditions and 2 year rainfall return period is compared to rainfall event with higher return period and lower soil moisture condition. Comparison between response of catchment to 2-year rainfall and fully saturated conditions and response to 50-year rainfall and field capacity conditions are presented in Figure 5.10. The resulting hydrographs show that low rainfall return period event with saturated conditions generates higher volume of discharge compared to a rainfall with 50-year return period and non-saturated soil moisture conditions.

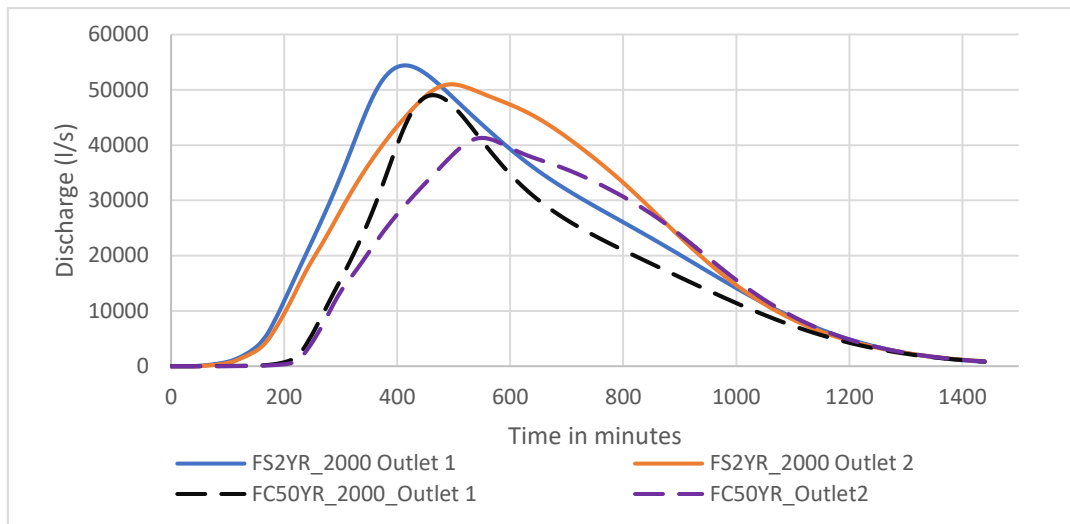


Figure 5.13 Response of catchment to rainfall with different return period and different soil moisture conditions

6. CONCLUSIONS AND RECOMMENDATIONS

6.1 Conclusions

The main objective of this study is to analyze the impact of soil moisture conditions on enhanced river discharge. Soil moisture data was collected in-situ to determine its spatial variability as well as to validate radar-retrieved soil moisture. The radar-retrieved soil moisture shows considerable underestimation of soil moisture conditions in the study area and are not found suitable to be used as initializing input in the event-based simulation. Using Boolean logic on the measured soil moisture values and characteristics of the area based on slope, land use and soil texture had produced a soil moisture map showing uniform soil moisture values in many parts of the catchment.

Open LISEM was used to analyze the effect of initial soil moisture and different rainfall characteristics on enhanced river discharge. The model was able to simulate different scenarios representing varying soil moisture and rainfall conditions. Results of the simulations show that response of catchment to a rainfall event is highly influenced by initial soil moisture conditions. Fully saturated soil moisture conditions show the highest amount of discharge, even higher than a rainfall event with 50 year return period and with soil moisture at field capacity.

The following sections answers the research questions posed in the Introduction

1. *What factors affect the accuracy of soil moisture map from SAR?*

Soil moisture map derived from radar shows high soil moisture values in south-west facing slopes of the catchment. The high values shown by the radar-retrieved soil moisture map at southwest slopes are caused by image distortion during radar image acquisition. The mode of sensing of radar instruments causes more illumination on one side of the slope, specially if the particular terrain is extremely rugged. The dense vegetation in the area also inhibits the penetration of radar energy into the ground surface. Rather, the radar wave encounters dielectric properties from canopy water content. The signal received by the radar antenna likely carries more signal from vegetation water content.

2. *What is the impact of topography to soil moisture?*

Measured soil moisture values between flat areas and sloping areas show variation with flat areas exhibiting lower soil moisture. Variation of soil moisture within the sloping areas however is not very significant. Slope gradients were divided between moderate slopes, where slope angle is between 5 and 20 degrees, and steep slopes where slope angle is greater than 20 degrees. Mean soil moisture in both gradient classification is $0.39 \text{ m}^3/\text{m}^3$. Standard deviation of soil moisture in moderate slopes is 0.07 and standard deviation in steep slopes is 0.05.

3. *What is the impact of land use to soil moisture?*

Measure soil moisture in land use shows distinct variation in its units. Dominant land use units present in the study area are grassland, cropland and forest. Mean soil moisture values measured among these units are 0.27, 0.41, and 0.36, respectively. Higher soil moisture values in cropland units is likely due to human interventions in the agricultural lands.

4. *Which catchment property contributes most to variance of soil moisture values?*

Based on the Boolean operation, used to give soil moisture values to different combinations of land use, soil texture and slope gradient, highest soil moisture amounts are found in classes with clay loam soil texture and lowest was found in sandy loam. Although it must be noted that classes with sandy loam soil texture also show relatively high soil moisture. The available information gathered from the field work is not

enough to determine which catchment property gives the highest variance. This may be due to the wet state of the catchment during the fieldwork which masks the soil moisture variabilities.

4. What is the response of the catchment in terms of peak discharge, total discharge and peak time to an extreme rainfall event given the driest soil moisture condition?

Extreme rainfall event with the driest soil moisture condition is characterized by a 50-year rainfall event with soil moisture at the wilting point. Catchment response at these conditions show a peak discharge at 17,800 l/s at Outlet 1 and 21,300 l/s at Outlet 2. Peak time at Outlet 1 is 437 minutes and 600 minutes at Outlet 2. Total discharge at Outlet 1 is 832,270 m³ and 991,660 m³ at Outlet 2. The same catchment response mentioned is similar to that of 20-year rainfall event with initial soil moisture at field capacity.

5. What is the response of the catchment to rainfall with low return period given the wettest soil moisture condition?

The scenario where there is lowest rainfall return period and wettest soil moisture conditions is characterized by 2-year rainfall event and fully saturated soil moisture conditions. These scenario generates a catchment response with peak discharge at Outlet 1 at 35,500 l/s and 38,900 l/s at Outlet 2. Peak time at Outlet 1 is 361 minutes and 427 minutes at Outlet 2. Total discharge at Outlet 1 is 1,740,000 m³ and 1,760,000 m³ at Outlet 2. This catchment response is larger than the scenario characterized by a high rainfall return period and soil moisture at wilting point condition.

6.2 Recommendations

Collection of in-situ soil moisture during the dry season can better show spatial soil signature and soil moisture variability compared to measuring soil moisture during the wet season. A well-distributed sample collection could be made by considering a smaller catchment with less terrain relief. A longer radar wavelength could be used to better sense soil moisture under tree canopy compared to 5.4 cm of C Band but errors induced by terrain are not likely to be solved by shifting to a longer radar wavelength.

Hydrological simulation could be improved by availability of measured discharge data. Rainfall variability should be considered specially because of the size of the catchment and its high relief. Rainfall data collected within the catchment itself will also greatly improve the performance of the model to closely simulate actual catchment processes.

REFERENCES

- Aqua Earth-observing satellite mission | Aqua Project Science. (n.d.). Retrieved July 26, 2017, from <https://aqua.nasa.gov/>
- Balenzano, A., Satalino, G., Lovergine, F., Rinaldi, M., Iacobellis, V., Mastronardi, N., & Mattia, F. (2013). European Journal of Remote Sensing On the use of temporal series of L-and X-band SAR data for soil moisture retrieval. Capitanata plain case study. *European Journal of Remote Sensing - European Journal of Remote Sensing*, 46(46), 721–737. <https://doi.org/10.5721/EuJRS20134643>
- Berthet, L., Andréassian, V., Perrin, C., & Javelle, P. (2009). How crucial is it to account for the antecedent moisture conditions in flood forecasting? Comparison of event-based and continuous approaches on 178 catchments. *Hydrology and Earth System Sciences Discussions*, (13), 819–831. Retrieved from <https://hal.archives-ouvertes.fr/hal-00583212/>
- Borah, D. K., Arnold, J. G., Bara, M., Krug, E. C., Liang, X.-Z., Borah, D. K. ; ... Bera, M. (2007). Storm Event and Continuous Hydrologic Modeling for Comprehensive and Efficient Watershed Simulations. <https://doi.org/10.1061/ASCE1084-06992007126605>
- Center for Research on the Epidemiology of Disasters (CRED). (2017). EMDAT-DB The International Disaster Database. Retrieved July 29, 2017, from http://emdat.be/emdat_db/
- Charpentier, M. A., & Groffman, P. M. (1992). Soil moisture variability within remote sensing pixels. *Journal of Geophysical Research*, 97(D17), 18987. <https://doi.org/10.1029/92JD00882>
- Das, K., & Paul, P. K. (2015). Present status of soil moisture estimation by microwave remote sensing. *Cogent Geoscience*, 1(1), 1–21. <https://doi.org/10.1080/23312041.2015.1084669>
- De Roo, A. P. J., Wesseling, C. G., & Ritsema, C. J. (1996). LISEM: A single-event physically based hydrological and soil erosion model for drainage basins I: Theory, input and output. *Hydrological Processes*, 10(8), 1107–1117. [https://doi.org/10.1002/\(SICI\)1099-1085\(199608\)10:8<1107::AID-HYP415>3.0.CO;2-4](https://doi.org/10.1002/(SICI)1099-1085(199608)10:8<1107::AID-HYP415>3.0.CO;2-4)
- Dingman, S. L. (1994). *Physical Hydrology*. (R. McConnin, Ed.) (First). Upper Saddle River, New Jersey: Prentice-Hall, Inc.
- Doubková, M., Van Dijk, A. I. J. M., Sabel, D., Wagner, W., & Blöschl, G. (2012). Evaluation of the predicted error of the soil moisture retrieval from C-band SAR by comparison against modelled soil moisture estimates over Australia. *Remote Sensing of Environment*, 120(2), 188–196. <https://doi.org/10.1016/j.rse.2011.09.031>
- Dunne, T. (1983). Relation of Field Studies and Modelling in the Prediction of Storm Runoff. *Journal of Hydrology*, 65, 25–48. Retrieved from https://www.researchgate.net/profile/Thomas_Dunne2/publication/245098726_Relation_to_Field_Studies_and_Modeling_in_the_Prediction_of_Storm_Runoff/links/55b02a7b08ae32092e06ff0b/Relation-to-Field-Studies-and-Modeling-in-the-Prediction-of-Storm-Runoff.pdf
- Entekhabi, D., Njoku, E. G., Houser, P., Spencer, M., Doiron, T., Yunjin Kim, ... van Zyl, J. (2004). The hydrosphere State (hydros) Satellite mission: an Earth system pathfinder for global mapping of soil moisture and land freeze/thaw. *IEEE Transactions on Geoscience and Remote Sensing*, 42(10), 2184–2195. <https://doi.org/10.1109/TGRS.2004.834631>
- Entekhabi, D., Rodriguez-Iturbe, I., & Castelli, F. (1996). Mutual interaction of soil moisture state and atmospheric processes. *Journal of Hydrology ELSEVIER Journal of Hydrology*, 184, 3–17. Retrieved from http://ac.els-cdn.com/0022169495029656/1-s2.0-0022169495029656-main.pdf?_tid=043e1342-471a-11e7-9502-00000aacb35e&acdnat=1496356452_853ff0a31f280f03254da1e7e0848df6
- Entekhabi, D., Rodriguez-Iturbe, I., & Castelli, F. (1996). Mutual interaction of soil moisture state and atmospheric processes. *Journal of Hydrology ELSEVIER Journal of Hydrology*, 184, 3–17. Retrieved from <http://ac.els-cdn.com/0022169495029656/1-s2.0-0022169495029656->

main.pdf?_tid=a0e5cd1e-463b-11e7-821d-00000aacb361&acdnat=1496260937_6f9af653e2ef777c511bdfb163c9e2a8

- ESA. (2007). InSAR Principles: Guidelines for SAR Interferometry Processing and Interpretation. Retrieved from https://www.esa.int/esapub/tm/tm19/TM-19_ptA.pdf
- Garcia-Estringana, P., Latron, J., Llorens, P., & Gallart, F. (2012). Spatial and temporal dynamics of soil moisture in a Mediterranean mountain area (Vallcebre, NE Spain). *Ecohydrology*, 6(5), n/a-n/a. <https://doi.org/10.1002/eco.1295>
- Hawley, M. E., Jackson, T. J., & McCuen, R. H. (1983). Surface soil moisture variation on small agricultural watersheds. *Journal of Hydrology*, 62(1–4), 179–200. [https://doi.org/10.1016/0022-1694\(83\)90102-6](https://doi.org/10.1016/0022-1694(83)90102-6)
- Hornacek, M., Wagner, W., Sabel, D., Truong, H.-L., Snoeij, P., Hahmann, T., ... Doubkova, M. (2012). Potential for High Resolution Systematic Global Surface Soil Moisture Retrieval via Change Detection Using Sentinel-1. *IEEE Journal of Selected Topics in Applied Earth Observations and Remote Sensing*, 5(4), 1303–1311. <https://doi.org/10.1109/JSTARS.2012.2190136>
- Introducing SMOS / SMOS / Observing the Earth / Our Activities / ESA. (n.d.). Retrieved July 26, 2017, from http://www.esa.int/Our_Activities/Observing_the_Earth/SMOS/Introducing_SMOS
- Jetten, V. (n.d.). openLISEM – a spatial model for runoff, floods and erosion. Retrieved March 14, 2018, from <https://blog.utwente.nl/lisem/>
- Jetten, V. (2014). A brief guide to openLISEM. Retrieved from [ftp://197.155.77.6/sourceforge/1/li/lisem/A brief guide to openLISEM 140702.pdf](ftp://197.155.77.6/sourceforge/1/li/lisem/A%20brief%20guide%20to%20openLISEM%20140702.pdf)
- Kornelsen, K. C., & Coulibaly, P. (2013). Advances in soil moisture retrieval from synthetic aperture radar and hydrological applications. *Journal of Hydrology*, 476, 460–489. <https://doi.org/10.1016/j.jhydrol.2012.10.044>
- Kuriakose, S. (2009). *Physically-based dynamic modelling of the effect of land use changes on shallow landslide initiation in the Western Ghats of Kerala, India Sekhar Lukeose Kuriakose*. University of Twente. Retrieved from http://www.itc.nl/library/papers_2010/phd/kuriakose.pdf
- Lofile, E., Kubionok, J. (1996). Landform development and bioturbation on the khora t plateau, northeast thailand. *Nat. Hist. Bull. Siam Soc.*, 44, 199–216.
- Loo, Y. Y., Billa, L., & Singh, A. (2015). Effect of climate change on seasonal monsoon in Asia and its impact on the variability of monsoon rainfall in Southeast Asia. *Geoscience Frontiers*, 6(6), 817–823. <https://doi.org/10.1016/j.gsf.2014.02.009>
- Malenovský, Z., Rott, H., Cihlar, J., Schaepman, M. E., García-Santos, G., & Fernandes, R. (2012). Sentinels for science: Potential of Sentinel-1, -2, and -3 missions for scientific observations of ocean, cryosphere, and land. *Remote Sensing of Environment*, 120, 91–101. <https://doi.org/10.1016/J.RSE.2011.09.026>
- Mohanty, B. ., & Skaggs, T. . (2001). Spatio-temporal evolution and time-stable characteristics of soil moisture within remote sensing footprints with varying soil, slope, and vegetation. *Advances in Water Resources*, 24(9–10), 1051–1067. [https://doi.org/10.1016/S0309-1708\(01\)00034-3](https://doi.org/10.1016/S0309-1708(01)00034-3)
- Moran, M. S., Peters-Lidard, C. D., Watts, J. M., Mcelroy, S., Moran, M. S., & Watts, J. M. (2004). Estimating soil moisture at the watershed scale with satellite-based radar and land surface models. *Can. J. Remote Sensing*, 30(5), 805–826. Retrieved from <https://naldc.nal.usda.gov/naldc/download.xhtml?id=6991&content=PDF>
- Penna, D., Tromp-Van Meerveld, H. J., Gobbi, A., Borga, M., & Dalla Fontana, G. (2011). The influence of soil moisture on threshold runoff generation processes in an alpine headwater catchment. *Hydrology and Earth System Sciences*, 15(3), 689–702. <https://doi.org/10.5194/hess-15-689-2011>
- Perkins, K. S., Nimmo, J. R., & Medeiros, A. C. (2012). Effects of native forest restoration on soil

- hydraulic properties, Auwahi, Maui, Hawaiian Islands. *Geophysical Research Letters*, 39(5), n/a-n/a. <https://doi.org/10.1029/2012GL051120>
- Saxton, K. E., & Rawls, W. J. (2006). Soil Water Characteristic Estimates by Texture and Organic Matter for Hydrologic Solutions. *Soil Science Society of America Journal*, 70(5), 1569. <https://doi.org/10.2136/sssaj2005.0117>
- Seneviratne, S. I., Corti, T., Davin, E. L., Hirschi, M., Jaeger, E. B., Lehner, I., ... Teuling, A. J. (2010). Investigating soil moisture–climate interactions in a changing climate: A review. *Earth-Science Reviews*, 99(3–4), 125–161. <https://doi.org/10.1016/j.earscirev.2010.02.004>
- Shrestha, A., Babel, M. S., Weesakul, S., & Vojinovic, Z. (2017). Developing Intensity-Duration-Frequency (IDF) curves under climate change uncertainty: The case of Bangkok, Thailand. *Water (Switzerland)*, 9(2). <https://doi.org/10.3390/w9020145>
- SMAP: Mission Description. (n.d.). Retrieved July 26, 2017, from <https://smap.jpl.nasa.gov/mission/description/>
- Solomon, H. (2005). *A GIS based Surface Runoff Modelling and Analysis of Contributing Factors*. University of Twente. Retrieved from http://www.itc.nl/library/papers_2005/msc/ereg/harssema.pdf
- UNISDR. (2015). *Making Development Sustainable: The Future of Disaster Risk Management. Global Assessment Report on Disaster Risk Reduction. International Strategy for Disaster Reduction (ISDR)*. <https://doi.org/9789211320282>
- Velde, R. Van Der, Salama, M. S., Eweys, O. A., Wen, J., & Wang, Q. (2015). Active / Passive Microwave Observations Over the East of the Netherlands, 8(9), 4355–4372.
- Wagner, W., Sabel, D., Doubkova, M., Bartsch, A., & Pathe, C. (2009). the Potential of Sentinel-1 for Monitoring Soil Moisture With a High Spatial Resolution At Global Scale, 2009(November 2009), 18–20.
- Western, A. W., Grayson, R. B., Bloschl, G., & Wilson, D. J. (2003). Spatial variability of soil moisture and its implications for scaling. In Y. Pachepsky, D. Radcliffe, & M. Selim (Eds.), *Scaling methods in soil physics* (pp. 119–139). Boca Raton: CRC Press.
- Yumuang, S. (2006). 2001 Debris flow and debris flood in Nam Ko area, Phetchabun province, central Thailand. *Environmental Geology*, 51, 545–564. <https://doi.org/10.1007/s00254-006-0351-9>
- Zribi, M., Kotti, F., Amri, R., Wagner, W., Shabou, M., Lili-Chabaane, Z., & Baghdadadi, N. (2014). Soil moisture mapping in a semiarid region, based on ASAR/Wide Swath satellite data. *Water Resources Research*, 50(2), 823–835. <https://doi.org/10.1002/2012WR013405>

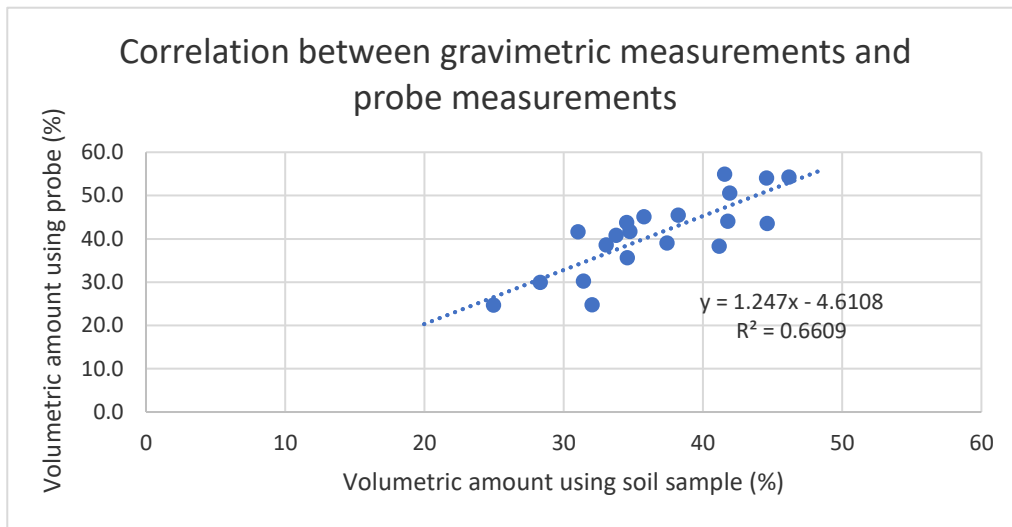
APPENDIX

Appendix A – Description of radar images used in soil moisture retrieval

Image Number	Date of Acquisition	Pass	Polarization	Rel Orbit	Orbit Cycle
1	10-Oct-16	Descending	VV VH	62	91
2	13-Oct-16	Ascending	VV	99	91
3	18-Oct-16	Descending	VV VH	172	91
4	22-Oct-16	Descending	VV VH	62	92
5	3-Nov-16	Descending	VV VH	62	93
6	6-Nov-16	Ascending	VV	99	93
7	11-Nov-16	Ascending	VV	172	93
8	15-Nov-16	Descending	VV VH	62	94
9	27-Nov-16	Descending	VV VH	62	95
10	30-Nov-16	Ascending	VV	99	95
11	9-Dec-16	Descending	VV VH	62	96
12	21-Dec-16	Descending	VV VH	62	97
13	24-Dec-16	Ascending	VV	99	97
14	29-Dec-16	Ascending	VV	172	97
15	2-Jan-17	Descending	VV VH	62	98
16	14-Jan-17	Descending	VV VH	62	100
17	26-Jan-17	Descending	VV VH	62	100
18	7-Feb-17	Descending	VV VH	62	101
19	22-Feb-17	Ascending	VV VH	99	102
20	6-Mar-17	Ascending	VV VH	99	103
21	11-Mar-17	Ascending	VV VH	172	103
22	15-Mar-17	Descending	VV VH	62	104
23	18-Mar-17	Ascending	VV VH	99	104
24	23-Mar-17	Ascending	VV VH	172	104
25	27-Mar-17	Descending	VV VH	62	105
26	30-Mar-17	Ascending	VV VH	99	105
27	8-Apr-17	Descending	VV VH	62	106
28	11-Apr-17	Ascending	VV VH	99	106
29	20-Apr-17	Descending	VV VH	62	107
30	23-Apr-17	Ascending	VV VH	99	107
31	28-Apr-17	Ascending	VV VH	172	107
32	2-May-17	Descending	VV VH	62	108
33	5-May-17	Ascending	VV VH	99	108
34	14-May-17	Descending	VV VH	62	109
35	17-May-17	Ascending	VV VH	99	109
36	22-May-17	Ascending	VV VH	172	109
37	26-May-17	Descending	VV VH	62	110
38	29-May-17	Ascending	VV VH	99	110
39	3-Jun-17	Ascending	VV VH	172	110
40	7-Jun-17	Descending	VV VH	62	111
41	15-Jun-17	Ascending	VV VH	172	111

42	19-Jun-17	Descending	VV VH	62	112
43	22-Jun-17	Ascending	VV VH	99	102
44	27-Jun-17	Ascending	VV VH	172	112
45	1-Jul-17	Descending	VV VH	62	113
46	4-Jul-17	Ascending	VV VH	99	113
47	9-Jul-17	Ascending	VV VH	172	113
48	13-Jul-17	Descending	VV VH	62	114
49	21-Jul-17	Ascending	VV VH	172	114
50	25-Jul-17	Descending	VV VH	62	115
51	6-Aug-17	Descending	VV VH	62	116
52	9-Aug-17	Ascending	VV VH	99	116
53	14-Aug-17	Ascending	VV VH	172	116
54	18-Aug-17	Descending	VV VH	62	117
55	21-Aug-17	Ascending	VV VH	99	117
56	26-Aug-17	Ascending	VV VH	172	117
57	30-Aug-17	Descending	VV VH	62	118
58	7-Sep-17	Ascending	VV VH	172	118
59	11-Sep-17	Descending	VV VH	62	119
60	14-Sep-17	Ascending	VV VH	99	119
61	19-Sep-17	Ascending	VV VH	172	119
62	23-Sep-17	Descending	VV VH	62	120
63	26-Sep-17	Ascending	VV VH	99	120

Appendix B – Comparison of soil moisture measurement using gravity method and Theta probe



Appendix C – Script for PCRaster

```
#! --matrixtable #! --lddin
#####
# Model: PCRaster for LISEM resampled at 30m #
# Date: 19 December 2017 #
# Version: 1.0 #
# Author: #
#####

binding
#####
### input maps ###
#####
DEM = dem30.map; #digital elevation model
mask = mask30.map;
veg = vc2000.map; #vegetation cover map from sat image resampled to nearest neighbor
LDD = ldd.map;
outlet=outlet.map;
landuse=lc30_2000.map; #land cover map resampled to nearest neighbor
lutable = lu.tbl; #1=plant height, 2=random roughness, 3=manning's, 4=ksat, 5=porosity
soilunit=soil.map; #soil cover map based on texture
soil_tbl = soil_n.tbl; #this table is based on soil texture classes
#1=texture, 2=field capacity, 3=wilting point, 4=thetas(porosity), 5=ksat(mm/h),
#6=psi:suction at wetting front(cm), 7=bulk density

#####
###output maps#####
#####

ksat1=ksat1.map; #ksat at 1st layer
thetas1=thetas1.map; #saturation at 1st layer
thetai1=thetai1.map; #initial soil moisture at 1st layer
psi1=psi1.map; #wetting front suction at 1st layer

theta_fc=theta_fc.map; #soil moisture at field capacity
theta_wp=theta_wp.map; #soil moisture at wilting point
theta_s=thetas2.map; #soil porosity
theta_i=thetai2.map; #initial soil moisture
ksat2=ksat2.map; #ksat at mm/hour
psi2=psi2.map; #suction at wetting front (cm)
BD = BD.map; #bulk density

ch=ch.map; #crop height
rr=rr.map; #random roughness
mann=n.map; #manning's number
per=per.map; #vegetation cover
lai=lai.map; #leaf area index
smax=smax.map; #storage capacity for interception

grad=grad.map; #slope in sine
id=id.map; #pluviograph influence zones
lddchan=lddchan.map; #channel 1D network
chanwidth=chanwidt.map; #channel width (m)
changrad=changrad.map; #channel gradient, sine
chanman=chanman.map; #channel manning
accuflux=accuflux.map; #accumulated material
chanmask=chanmask.map;
chanside = chanside.map;
soildepth1=sdepth1.map;
soildepth2=sdepth2.map;
```

```

channeldist=channeldist.map;
drain=drains.map;

areamap
mask30.map;

initial

## Infiltration 1st layer

report ksat1 = lookupscalar(lutable, 4, landuse)*mask;
#ksat in first column based on landuse
report psi1 = lookupscalar(soil_tbl, 6, soilunit);
#suction at wetting front
report thetas1= lookupscalar(soil_tbl, 4, soilunit)*mask;
#porosity
report thetai1 = thetas1*0.75;
#initial soil moisture

### Infiltration 2nd layer

report theta_fc = lookupscalar(soil_tbl, 2, soilunit);
# field capacity in column 2 (-)
report theta_wp = lookupscalar(soil_tbl, 3, soilunit);
# wilting point in column 3 (-)
report theta_s= lookupscalar(soil_tbl, 4, soilunit);
# porosity in column 4 (-)
report ksat2 = lookupscalar(soil_tbl, 5, soilunit);
# ksat in column 5
report psi2 = lookupscalar(soil_tbl, 6, soilunit);
#suction at wetting front at column 6
report theta_i = theta_s*0.5;
#initial soil moisture conditions

### Land use
report per= if(((landuse eq 5) or (landuse eq 11) or (landuse eq 8) and (vegclt lt 30)), 0.9, vegclt/100);
# constant plant cover (-)
report ch = lookupscalar(lutable, 1, landuse)*mask;
# plant height (m)
report rr = lookupscalar(lutable, 2, landuse)*mask;
# random roughness
report mann = lookupscalar(lutable, 3, landuse)*mask;
# manning's coefficient
lai = ln(1-min(per,0.99))/-0.4;
report lai = if(per gt 0, lai/per, 0);

####catchment
slope = slope(DEM);
report grad = sin(atan(slope(DEM)));
#sine gradient
curv = profcurv(DEM);
#profile curvature calculation; negative at concave, positive at convex

###channel properties

report LDD = lddcreate(DEM, 1e20, 1e20, 1e20, 1e20);
report outlet.map = pit(LDD);
stream = streamorder(LDD);
#drains = if(stream gt 0, stream, 0);
report chanmask = if(stream gt 0, 1, 0)*mask;

```

```

#creates missing values outside of channels

report lddchan = lddcreate(DEM*chanmask,1e31,1e31,1e31,1e31);
#creates ldd for stream channels
report outpoint.map = cover(scalar(pit(lddchan)),0)*mask;

report changrad = sin(atan(slope(DEM*chanmask)));
# channel slope

report chanman = mann*chanmask;
#channel manning's
report chanside = chanmask*scalar(0);
# rectangular channel

accuflux = accuflux(LDD, 1.0);
report chanwidth = chanmask * max(0.01, (0.2 + 4.5 * (accuflux.map - 2000)/(29000)));
#channel width determined in relation to discharge

report channeldepth = chanmask * (0.1 + 3 * (accuflux.map - 2000)/(29000));
report channeldist = spread(nominal(chanmask),0,0,1.0);
#friction over channels

###vegetation parameters

smax_crop = if(landuse eq 13 or landuse eq 14, 0.935+(0.498*lai)-(0.00575*sqr(lai)),0);
smax_forest = if(landuse eq 4 or landuse eq 5 or landuse eq 8 or landuse eq 10 or landuse eq 11,0.2858*(lai),0);
smax_needleleaf = if(landuse eq 9, 0.2331*(lai),0);
smax_bare_hardsurfaces = if(landuse eq 1 or landuse eq 12 or landuse eq 17 or landuse eq 18,0.001,0);
report smax.map = smax_crop + smax_forest + smax_needleleaf + smax_bare_hardsurfaces;

###soil depth

soildepth1 = (max(1.0,3.7*(30.083 - 0.00143 * DEM - 0.00062 * channeldist - 2.6718 * abs(slope) - 2.746 *
curv)))/4;
soildepth2 = (max(1.0,3.7*(30.083 - 0.00143 * DEM - 0.00062 * channeldist - 2.6718 * abs(slope) - 2.746 *
curv)))/2;
report soildepth1= 50* windowaverage(soildepth1,20.0);
report soildepth2= 50* windowaverage(soildepth2,20.0);

```